AGU PUBLICATIONS

JGR

Journal of Geophysical Research: Planets

RESEARCH ARTICLE
10.1002/2017JE005293

Key Points:
- Martian analogues are still needed to understand the surface of Mars and interpret the data received from rovers and landers
- The Qaidam Basin contains many geomorphological structures and mineral materials comparable to those of modern Mars
- The remarkable similarities make the Qaidam Basin a potential valuable Martian analogue to study modern geomorphic processes on Mars

Correspondence to:
Y. Li,
yiliang@hku.hk

Citation:
Anglés, A., and Y. Li (2017), The western Qaidam Basin as a potential Martian environmental analogue: An overview, *J. Geophys. Res. Planets*, *122*, 856–888, doi:10.1002/2017JE005293.

Received 9 MAR 2017
Accepted 5 APR 2017
Accepted article online 28 APR 2017
Published online 21 MAY 2017

The western Qaidam Basin as a potential Martian environmental analogue: An overview

Angélica Anglés[1] and Yiliang Li[1]

[1]Department of Earth Sciences, The University of Hong Kong, Hong Kong

Abstract The early Martian environment is interpreted as warmer and wetter, before a significant change in its global climatic conditions irreversibly led to the current hyperarid environments. This transition is one of the most intriguing processes of Martian history. The extreme climatic change is preserved in the salt deposits, desiccated landscapes, and geomorphological structures that were shaped by the evaporation of water. However, until a manned journey to Mars is feasible, many Martian materials, morphological structures, and much of its evolutionary history will continue to be poorly understood. In this regard, searching and investigating Martian analogues are still meaningful. To find an Earth environment with a whole set of Martian structures distributed at a scale comparable to Mars is even more important to test landing crafts and provide optimized working parameters for rovers. The western Qaidam Basin in North Tibetan Plateau is such a Martian analogue. The area harbors one of the most extreme hyperarid environments on Earth and contains a series of ancient lakes that evaporated at different evolutionary stages during the rise of the Tibetan Plateau. Large quantities of salts and geomorphological features formed during the transition of warmer-and-wet to colder-and-dry conditions provide unique references to study the modern Martian surface and interpret the orbital data. We present numerous similarities and results of investigations that suggest the Qaidam Basin as a potential analogue to study modern geomorphic processes on Mars, and suggest that this is an essential site to test future Mars sample return missions.

Plain Language Summary Martian evolutionary history is reflected in its landscape and geomorphological features, indicating that despite the extreme current hyperarid conditions, liquid water flowed on its surface well over 3.9 billion years ago. Despite the great amount of data available today, unless the geomorphological features can be studied in situ, we still need analogues here on Earth to better understand the dramatic climatic change on Mars and if the current conditions are suitable for microbial life to exist. We propose that the Qaidam Basin, in northwestern Tibetan Plateau, is a potential Martian analogue that can give us insight to unfold clues to study the Martian modern environments. The Qaidam Basin is the highest desert on Earth and harbors very similar extreme conditions that those on Mars today. We present our results from expeditions to the Qaidam Basin and compare them with Martian equivalents. The similarities between the Qaidam Basin and Mars are described in a context that suggest that this area is an essential site to test future Mars exploration missions.

1. Introduction

The most remarkable differences between the modern Earth and Mars is the various water-involved geological and climatic cycles on Earth that are absent on Mars due to the extremely arid and dry environment [*Blondel and Mason*, 2006]. The Martian climate, however, was once governed by similar hydrodynamic processes as that on Earth, despite the difference in atmospheric composition and mean surface pressure [*Read and Lewis*, 2004]. Since their discovery by the Mariner 9 and Viking missions, a number of morphological structures, such as river channels or valley networks, raised speculations that the early Martian climate, most likely until the Noachian or even early in the Hesperian epoch, was wet and warm [*Blondel and Mason*, 2006; *Kargel*, 2004]. Minerals, such as sulfates, carbonates, chlorides, and clays closely related to aqueous environments, have been detected on different locations [*Arvidson et al.*, 2005; *Bishop et al.*, 2008; *Ehlmann et al.*, 2008; *Murchie et al.*, 2009], confirming that water was stable at certain surface conditions. But the strong solar winds from the young Sun 4 billion years ago resulted in the escape of atmospheric gases to space [*Cabrol and Grin*, 2010; *Carr*, 1996; *Connerney et al.*, 1999], that consequently changed the climate irreversibly to the present cold, windy, and dry conditions [*Jakosky et al.*, 2015]. The solar wind bombardment and resulted loss of atmospheric gases were the main processes for the Martian climate change [*Jakosky et al.*, 2015],

which resulted in a catastrophic drought with the disappearance of the ancient water bodies on Mars [*Di and Hynek*, 2010], leaving behind the large quantities of saline deposits.

Recent space and in situ Martian explorations suggest a dynamic climate that varies on timescales of tens of millions of years [*Blondel and Mason*, 2006; *Head et al.*, 2003]. Spacecraft missions provide strong evidence that Mars has not always been the cold and dry planet as it is today but rather has undergone dramatic shifts of wide timescales since 3.9 billion years [*Blondel and Mason*, 2006; *Masursky et al.*, 1977]. Those lines of evidence include morphological features observed from space and more detailed geological formations identified by several landed rovers, such as polygons, gullies, mass debris flows, and landforms that have been developed by recent episodic hydrodynamic processes. This evolution is widely recorded by the erosional discontinuities, fluvial networks, and sedimentary layering, with some of these structures well-preserved nowadays [*De Silva et al.*, 2010; *Irwin et al.*, 2005; *Levy et al.*, 2009a]. However, understanding the hydrologic history and climate of Mars continues to be a challenge. Although rovers have covered several kilometers of Mars over many years, their surveys are limited to the narrow belt within their visual range. The rovers are engineered to travel in distances of tens of kilometers and collect information along their pathways of a few meters wide on Martian terrain. Relatively large-scale geological structures (meters to kilometers), which are important in understanding Martian geological processes, are out of the rovers' reach. Currently, these large-scale structures can only be studied based on images from orbiting spacecrafts, which, however, cannot provide high enough resolutions for detailed mineralogical compositions or related geochemical processes. Unless these structures can be studied directly, the solution may still rest on comparisons of suitable terrestrial analogues with similar recent features created by hyperarid conditions.

To interpret the wide diversity of geomorphological features on Mars, there is a need for terrestrial analogues that are shaped by processes that modify the surface in arid regions or polar regions and are characterized by tectonic, volcanic, and impact processes, all of them simulating specific conditions of Mars. The potential habitable niches on Mars [*Dohm et al.*, 2011] also encourage investigations into terrestrial analogues for biological studies [*Komatsu and Ori*, 2000]. A number of terrestrial analogues for modern geomorphic processes on Mars have been proposed in recent literatures. For instance, deserts sites, where geomorphologies are comparable to those identified on Mars, could provide valuable information about the ancient climate and potential habitability on Mars. North Africa [*Paillou and Rosenqvist*, 2003; *Essefi et al.*, 2014b, 2014a], the western U.S. region [*Baldridge et al.*, 2004; *Chan et al.*, 2016], Atacama desert [*Houston*, 2006], or Western and Central Australia [*Bourke and Zimbelman*, 2001; *Brown et al.*, 2005] are good analogues to compare geomorphic processes and landforms, such as aeolian deposits, yardangs, or polygonal terrains. Other terrestrial analogues in polar regions are examined to assess physical and biological processes related to hyperarid and cold environments on Mars [*Osinski*, 2007; *Marchant and Head*, 2007; *Pollard et al.*, 2009; *Levy et al.*, 2009a; *Head and Marchant*, 2014]. Additionally, other terrestrial analogues have focused on specific aspects of Mars, such as valley networks [*Howard et al.*, 1987], impact crater lakes [*Komatsu et al.*, 2014], catastrophic flooding [*Baker and Nummedal*, 1978], or mineralogy [*Benison and LaClair*, 2003; *Fernández-Remolar et al.*, 2005; *Squyres et al.*, 2004; *Benison*, 2006]. However, taking into consideration the modern environmental conditions of Mars (hyperarid, low temperatures, strong aeolian processes, and high UV radiation), the current terrestrial analogues do not include all conditions of Mars. Supplementary analogue sites are required to comprehend the expansive and dynamic environmental conditions on Mars.

The western Qaidam Basin, a remote area in the north of Tibetan Plateau, is a promising Martian analogue site. The basin contains many geomorphological structures at a variety of scales and mineral materials comparable to features that started to form at the critical, rapid evolutionary stage that built the modern Martian environments. A few previous studies already proposed the Qaidam Basin as a terrestrial analogue [*Mayer et al.*, 2009; *Wang and Zheng*, 2009, *Zheng et al.*, 2009, 2013; *W. G. Kong et al.*, 2013, 2014; *Xiao et al.*, 2016]. However, the Qaidam Basin offers a more extensive range of characteristics for comparative studies of Mars than previously stated. Although there are environmental differences between the Qaidam Basin and the modern Mars (and even ancient Mars), the Qaidam Basin can serve as a good potential analogue site to compare modern geomorphic processes. We present a wide diversity of Martian sites, and although they might be distant from each other and even separated in time, we believe that those comparisons provide rich evidence that the Qaidam Basin is a suitable analogue to study modern Mars-like geomorphologies.

Table 1. Summary of Locations of Geomorphological Structures From the Qaidam Basin and on Mars for Comparisons

	The Qaidam Basin		Mars	
Geomorphological Structures	Figure No.	Location	Location	Figure No.
Catastrophic debris flows	Figure 6a	38.08°N, 91.88°E	6.6°S, 70.9°W	Figure 6d
	Figure 6b	38.08°N, 91.88°E		
	Figure 6c	38.08°N, 91.88°E		
Polygonal terrains	Figure 7a	38.75°N,91.75°E	125.74°W, 68.21°N	Figure 7d
	Figure 7b	38.73°N, 91.64°E	46.7°N, 117.5°E	Figure 7e
	Figure 7c	38.75°N, 91.75°E	62.61°S, 78.77°E	Figure 7f
Hollows and pits	Figure 9a	38.67°N, 91.17°E	5.4°S, 137.8°E	Figure 9d
	Figure 9b	38.32°N, 91.2°E	46.9°N, 117.36°E	Figure 9e
	Figure 9c	37.64°N, 94.99°E	50°S, 358.5°W	Figure 9f
Cyclic vertical accretion	Figure 10a	38.75°N, 91.74°E	21.1°S, 8.5°E	Figure 10b
Recurring Slope Lineae	Figure 11a	38.16°N, 91.34°E	32.04°S, 140.80°E	Figure 11b
Gullies	Figure 12a	38.32°N, 91.27°E	40.8°S, 201.9°E	Figure 12c
	Figure 12b	38.32°N, 91.27°E	1.5°S, 202.9°W	Figure 12d
			4.7°S, 298.6°E	Figure 12e
Light-toned gullies	Figure 13a	38.58°N, 95.14°E	47.2°S, 355.8°W	Figure 13b
Gullies and polygons	Figure 15a	38.57°N, 91.95°E	58.74°N, 82.38°E	Figure 15b
Fluvial valleys and alluvial fans	Figure 16a	39.16°N, 92°E	7.5°N, 33°W	Figure 16c
	Figure 16b	39.16°N, 92°E	4.6°S, 137.43°E	Figure 16d
Yardangs	Figure 17a	37.61°N, 92.23°E	2.83°N, 147.64°E	Figure 17d
	Figure 17b	37.71°N, 92.58°E	5.08°S, 137.85°E	Figure 17e
	Figure 17c	38.31°N, 90.81°E		
Wind streaks	Figure 19a	38.89°N, 92.29°E	8.17°N, 297.39°W	Figure 19f
	Figure 19b	38.79°N, 92.33°E		
	Figure 19c	38.49°N, 92.40°E		
	Figure 19d	38.48°N, 92.28°E		
	Figure 19e	38.76°N, 92.42°E		
Gravel deposition	Figure 20a	38.33°N, 90.79°E	5.24°S, 137.18°E	Figure 20d
	Figure 20b	38.33°N, 90.79°E		
	Figure 20c	38.33°N, 90.79°E		
Dune fields	Figure 21a	38.37°N, 91.63°E	83°50′S, 118°70′W	Figure 21c
	Figure 21b	38.15°N, 91.19°E	13.9°S, 59.2°W	Figure 21d
Swirling textures	Figure 22a	37.72°N, 92.88°E	40°S, 52°E	Figure 22b
Ring structures	Figure 23a	38.49°N, 91.74°E	85.70°N, 21.00°W	Figure 23b

Due to the ease of access for expeditions and the higher density of geomorphological features similar to Mars, we focused our study on the western area of the basin. Here we generally refer to the "Qaidam Basin" as more specifically the western region studied. In order to describe the comparable structures in the Qaidam Basin and on Mars from the same point of view, we have endeavored to compare data from similar sources, such as Google Earth images of the Qaidam Basin compared with images from Martian orbital crafts (Table 1). The main aim of this study is to present the geomorphologies of the Qaidam Basin as analogues of modern geomorphic features on Mars. We also present general similarities in mineralogy, climatic conditions, and evolutionary history between the Qaidam Basin and Mars. In order to raise more comparative planetary studies in this area, we complement the comparisons with the results of mineralogical investigations of the evaporate deposits of the Qaidam Basin. In this pilot study, comparisons are made with observed Martian structures, the similarities are presented broadly, and the geology of structures and processes that mimic contemporary epochs of Mars are described in a context that suggest the Qaidam Basin as a potential Martian analogue.

2. Regional Geological Setting

The Qaidam Basin lies in the north of Tibetan Plateau (Figure 1) [*Anglés and Li*, 2016], measuring roughly 850 km from east to west and 150–300 km from north to south [*Fang et al.*, 2007], covering a total area of 120,000 km^2 and a catchment area of 250,000 km^2 [*Kezao and Bowler*, 1986]. The basin is comprised by the monumental Altyn-Tagh strike-slip fault in the northwest, the Qilian-South Mountain Zongwulong strike-slip fault in the northeast, the Ela Mountain to the east, and the Qiman-Tagh-Kunlun Mountain

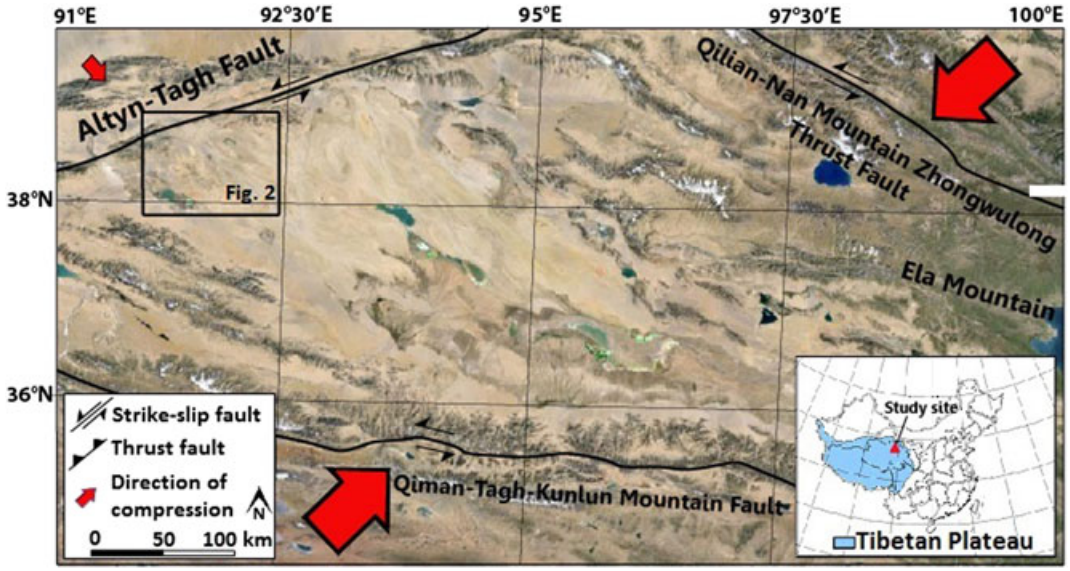

Figure 1. Tectonic configuration of northwest Tibetan Plateau and its surrounding mountains and faults. The directions of compression of Qiman-Tagh-Kunlun Mountain Fault, Altyn-Tagh Fault, and Qilian-Nan Mountain-Zhongwulong Fault are indicated with red arrows [*Anglés and Li*, 2016].

strike-slip fault to the south [*Fang et al.*, 2007]. The compressional forces between the Qilian-South and the Qiman-Tagh-Kunlun Mountain faults are in the NE-SW direction where the force between the Altyn-Tagh fault and Ela Mountain is in the NW-SE direction.

The formation of the Qaidam Basin can be traced back to the Jurassic, when the vast majority of the Tibetan Plateau was an enormous giant lake [*Zheng*, 1997]. Due to the ongoing Indo-Asian collision, two main thrust systems were initiated: an older system in the north of the plateau initiated in the Paleocene and a younger one in the southern side initiated in the Oligocene [*Yin et al.*, 2008]. The Qaidam Basin has been since at least the Oligocene an internally drained basin [*Yin et al.*, 2008]. From the Miocene to the Pleistocene, the area expanded and migrated northwest-southeast due to highly irregular periods of uplift and deformation in the northwestern part [*Yin et al.*, 2008]. The continuous and intense collisional-compressional tectonic activities eventually resulted in an uneven floor that broke the giant lake into smaller ones [*Zheng et al.*, 1993; *Zheng*, 1997].

As a result of the rise of the Tibetan Plateau, atmospheric circulation underwent differential changes that caused drastic climatic variations and a gradual transformation of these lakes to completely dry and saline basins [*Zheng*, 1997]. The basin today preserves a full record of Cenozoic sedimentation [*Yin et al.*, 2008], with only a few small lakes in the center of the basin that still contain standing water. During the late Pliocene, the surface of the Qaidam Basin reached an average altitude of 3000 m with neighboring mountains up to 5000 m above sea level [*Zheng*, 1997] (Figure 2). The Qaidam Basin is the highest desert on Earth and the largest sedimentary basin in the Tibetan Plateau [*Zheng et al.*, 1993].

The high elevation eventually resulted in a hyperarid climate that consists of low-mean annual temperatures (average low ~1.9°C, average high ~12.6°C [*Wei et al.*, 1993]), 50–60°C of annual temperature difference [*Wei et al.*, 1993], tremendous diurnal temperature fluctuations (~27°C as the maximum temperature recorded at daytime [*F. J. Kong et al.*, 2013] and ~ −37°C at nighttime [*Wei et al.*, 1993]), 50% of sea level atmospheric pressure [*F. J. Kong et al.*, 2013], 67% of solar radiation exposure [*Wei et al.*, 1993], annual relative humidity of 30% [*F. J. Kong et al.*, 2013], very low annual average precipitation [<14 mm, *F. J. Kong et al.*, 2013], and extremely high average annual evaporation (3000–3200 mm [*Kezao and Bowler*, 1986]). The duration of the warm-cold transition in the water bodies, changes in the salinity from fresh to saline, and the transformation from large water bodies to dry playas in the Qaidam Basin is so long that the basin is unique among lake basins in the world [*Zheng*, 1997]. It is also the largest basin on the Tibetan Plateau [*Métivier et al.*, 1998; *Meyer et al.*, 1998; *Tapponnier et al.*, 2001], with possibly the world's thickest fluvio-lacustrine sedimentary deposits extending up to 12,000 m [*Fang et al.*, 2007].

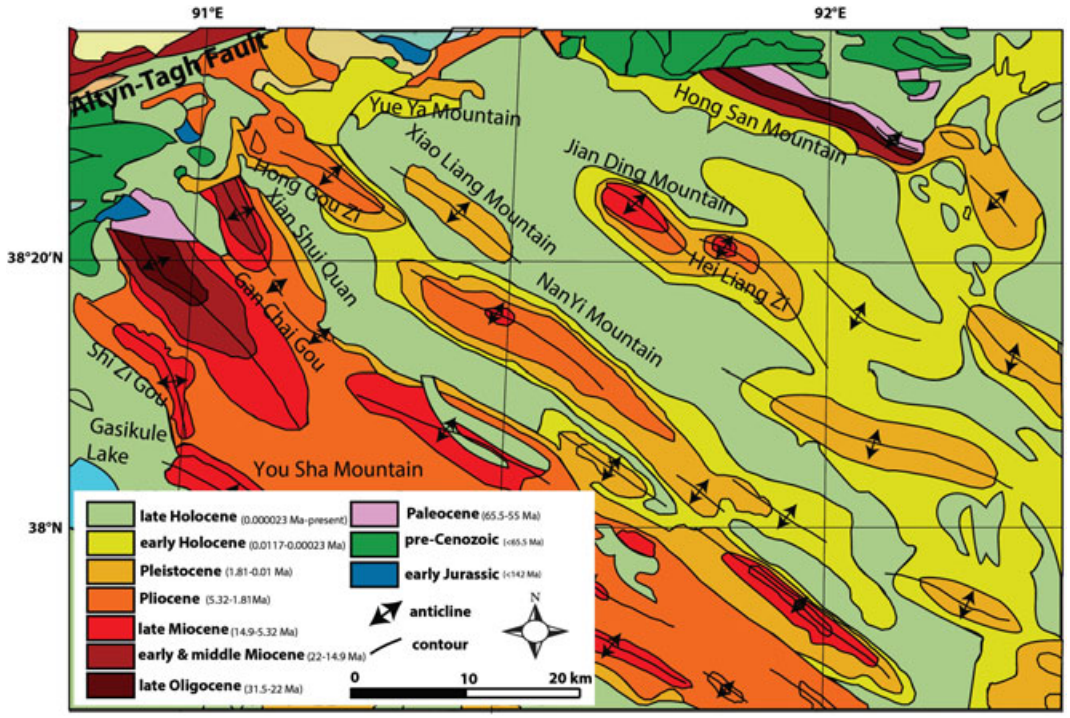

Figure 2. Western Qaidam Basin. Age and distribution of dry lakes and mountains in western Qaidam Basin. The different colors indicate the age [modified from *Qi and Fengqing*, 2007].

Qaidam, in Mongolian, means "salt flat," a description in agreement with the large amounts of salt deposits in the basin [*Kezao and Bowler*, 1986]. The entire basin floor is covered by hundreds of meter-thick evaporative salty crusts, where sulfate deposits dominate. Sulfate rich-minerals such as gypsum together with halite are the main minerals. The much higher abundance of sulfates in the area compared to the abundance of carbonates indicates that at least some of the water involved in their formation was sulfate-rich. The hyperarid environment makes the region uninhabitable by vegetation, where only evaporate crusts cover the surface (Figure 3).

The dried lakes are evidence of the different evolutionary stages of an area that once contained a body of water changed to an extremely dry environment; the high altitude is similar to the low atmospheric pressure on Mars and approximates the amount of solar radiation in the Martian surface; the hyperarid conditions provide means to study biosignatures in extreme environments; the large aeolian geologic features indicate that wind, instead of water, is the dominant sediment transport and erosion factor; and the wide variety of evaporate salts all provide clues that collectively point to the western Qaidam Basin as a suitable analogue site to provide promising study cases for investigating present Mars-like environments. In this contribution, the Qaidam Basin may shed light on studying the present hyperarid Martian environments.

3. Sample Collection and Analysis

3.1. Field Work

Field investigations of nine sites were conducted in the western Qaidam Basin during a 10 day expedition in August 2016, when the temperatures were at their highest. A total of 78 samples were collected from the nine different locations (Figure 4). Due to the enormous size of the Qaidam Basin, different routes were planned to visit the most significant geomorphic features. For instance locations A–D, although close to each other, were chosen as locations due to their high amount of yardangs, dunes, and ring structures. In location E habitable niches were found, and locations F–I were chosen because of the high density of gullies and recurring slope lineae in the high-altitude areas and polygonal terrains in the alluvial fans. The city of Huatugou was used as a baseline for the expedition. The samples were sealed in sterilized bags and stored at low temperature to avoid dehydration/rehydration changes. At the end of the expedition they were transported to the

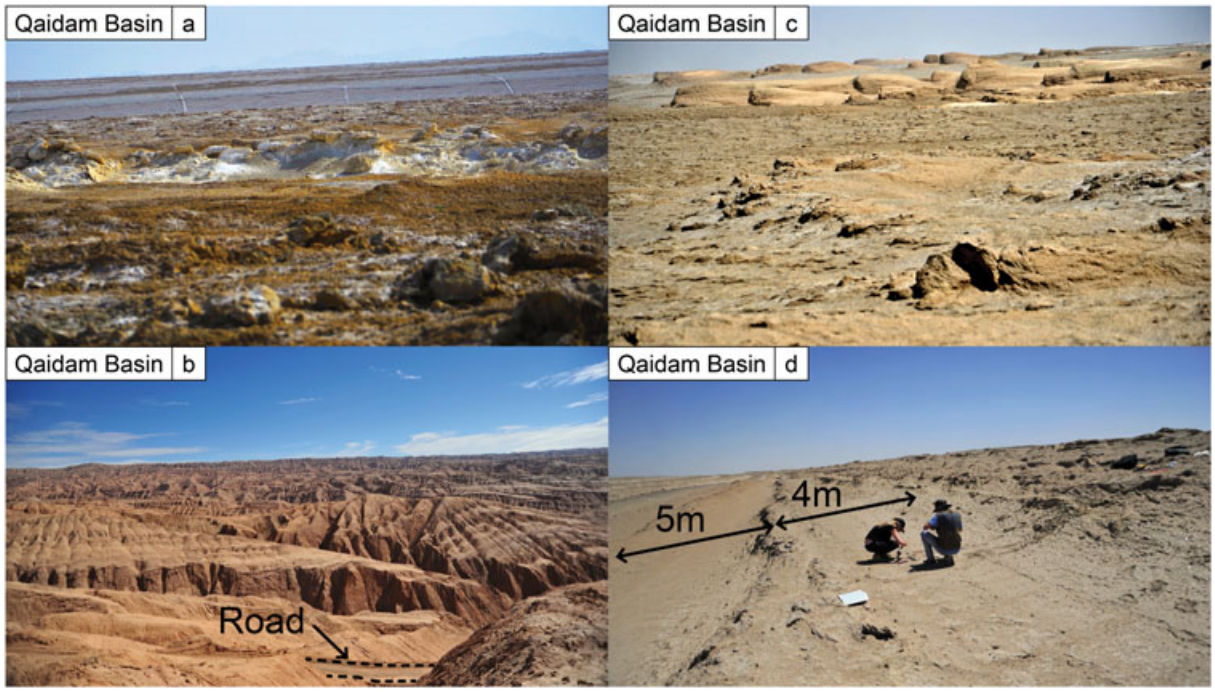

Figure 3. Typical morphologies of the Qaidam Basin. (a) Picture taken near the playa area of Xiaoliang Mountain, where the very weak hydrodynamic processes have eroded the surface. Note the track traces in the back of the picture for scale. (b) Mountain area in western Qaidam Basin near 38.10°N, 91.05°E. Note the road for scale. (c) Yardangs near Nanyi Mountain in the distance and salt and clay mixed playa. The yardangs are approximately 10 m high. (d) Image taken in the south part of Nanyi Mountain at 38.10°N, 91.75°E, at 2796 m of altitude.

Guangzhou Institute of Geochemistry for analysis. Global Positioning System information was annotated for each location, including full sample identification, date of collection, and a complete record of pictures in combination with geomorphic observations. Samples with potential biomass underneath were also collected for further analysis.

3.2. Analysis of Samples

Analyses of samples were carried out at the University of Hong Kong and Guangzhou Institute of Geochemistry, China. The majority of the samples were dry and formed by loose sediment; however, several samples showed noticeable water contents. They were therefore dried in an oven at ~50°C. The samples were then studied by means of scanning electron microscope and X-ray diffraction. Thermogravimetric analysis of three pure gypsum samples was performed in order to determine the magnitude of water content in the samples.

3.2.1. Scanning Electron Microscope

The original samples were initially analyzed with scanning electron microscope (SEM)-EDX (electron dispersive X-ray spectroscopy) using a Hitachi S-4800 scanning electron microscope to estimate the rough mineralogical assemblages in each sample. The samples were mounted on a stub of metal. After an Au-coating treatment, the samples were observed under secondary electron model at 5 kV. The typical collection time for the EDX analysis of each sample was ~1 min. No SEM results are presented here; however, we refer to them in the mineralogical identification of samples in Table 2.

3.2.2. X-ray Diffraction

Clay mineral separation from bulk rock samples and preparation of oriented sample mounts was carried out for analysis by X-ray diffraction (XRD) in order to characterize the clay minerals present in the samples. The method used was based on the Stokes' law settling of particles in a solution. For mineral characterization, the samples were ground by hand using a pestle and an agate mortar. The powdered samples were sieve-filtered to obtain a minimum grain size between 50 and 53 μm. Twenty grams for each powdered sample was suspended in approximately 600 mL of deionized water. The samples were then disaggregated for about 15 min at approximately 200 W with an ultrasonic probe. The samples were later placed on a

	A	B	C	D	E	F	G	H	I
latitude	38.05°N	38.06°N	38.07°N	38.09°N	38.11°N	38.33°N	38.45°N	38.47°N	38.59°N
longitude	91.83°E	91.82°E	91.73°E	91.75°E	91.05°E	90.80°E	91.25°E	91.21°E	91.01°E
altitude	2823 m	2821 m	2781 m	2769 m	3115 m	2993 m	2721 m	2772 m	3168 m
anhydrite					5%		10%		
blodite									20%
calcite			5%		2%	10%		5%	23%
clinochlore				14%	20%	15%	4%	3%	3%
dolomite							36%		
epsomite								19%	
glauberite							7%	13%	
gordonite						3%			
gypsum	6%	25%	22%				12%		
halite	29%	58%		56%		23%	13%		10%
illite				8%					
kainite								42%	
muscovite			7%	4%	5%	2%	2%	2%	2%
pentahydrite					15%	10%			
polyhalite		12%			12%				
polyhalite									
quartz	65%	5%	51%	18%	41%	37%	16%	16%	36%
thenardite			15%						6%

Figure 4. Location and abundance of mineral samples from the Qaidam Basin. The table below the image shows the locations and abundance of minerals found in each visited location of the Qaidam Basin.

stable surface to allow them to settle gravitationally overnight. This allowed sedimentation of all particles <2 μm. The supernatant was later poured off into centrifuge tubes to separate the fine clays by centrifugation at a centrifugal force of 1957 g. The fine clay sediment fractions were later placed on a hotplate to evaporate the remaining liquid completely. For the preparation of oriented mounts, the clay mineral fractions were suspended into small amounts of deionized water in glass slides and placed on a leveled and stable hot surface until the samples were completely dried and ready for X-ray diffraction analysis.

XRD analysis was carried out on an automated X-ray diffractometer Y500 (CDRIG Ltd.) with a nine-position sample charger and monocromated CuK_{α} radiation at the wavelength of 1.54 Å. The XRD patterns were scanned in the range of 3–80° 2Θ values. The peaks were refined by the Rietveld Refinement method by the software Materials Data JADE. The Rietveld Method was used as the differences between the calculated and the observed patterns of the samples can be minimized by a refinement procedure that uses a least squares algorithm. The observed diffraction patterns were then fit with calculated patterns. The background was removed manually for each sample to obtain a clearer pattern. The refinement strategy was followed by the chi-square goodness of fit. Once the crystallographic phase parameters were refined for all specimens, the weight fractions were calculated. The software JADE then defined the quantitative phase analysis of minerals, using its database of >400 phase entries. The XRD

Table 2. Minerals Identified in Materials of This Study

Mineral	Chemical Formula
Gypsum	$CaSO_4 \cdot 2H_2O$
Quartz	SiO_2
Aragonite	$CaCO_3$
Calcite	$CaCO_3$
Dolomite	$CaMg(CO_3)_2$
Halite	NaCl
Clinochlore	$(Mg_5Al)(AlSi_3)O_{10}(OH)_8$
Muscovite	$KAl_2(AlSi_3O_{10})(F,OH)_2$
Polyhalite	$K_2Ca_2Mg(SO_4)_4 \cdot 2H2O$
Anhydrite	$CaSO_4$
Pentahydrite	$MgSO_4 \cdot 5H_2O$
Sanderite	$MgSO_4 \cdot 2H_2O$
Thenardite	Na_2SO_4
Epsomite	$MgSO_4 \cdot 7H_2O$
Gordonite	$MgAl_2(PO_4)_2(OH)_2 \cdot 8H_2O$
Illite	$(K,H_3O)(Al,Mg,Fe)_2(Si,Al)_4O_{10}[(OH)_2,(H_2O)]$
Glauberite	$Na_2Ca(SO_4)_2$
Kainite	$KMg(SO_4)Cl \cdot 3H_2O$
Blodite	$Na_2Mg(SO_4)_2 \cdot 4H_2O$

patterns were dominated by sharp gypsum and halite peaks, with broad clay peaks. Some of the samples displayed intense clay peaks.

Although we found that this method worked well for the majority of specimens, we understand that our results are only a rough estimate of reality. Although the major mineral phases identified by XRD were consistent with SEM data, some minor features could not be identified with these methods and will require a more detailed analysis. More samples and different quantification approaches will be used in the future for the clay mineral characterization of the Qaidam Basin samples. Table 2 displays the chemical formulae of the minerals identified by SEM and XRD in this study.

Figure 4 shows the minerals identified in the sampling locations in western Qaidam Basin. Halite dominates in almost all analyzed samples, indicating that the sulfate brines were saturated in Na and Cl. Quartz, calcite (or dolomite), muscovite, clinochlore, and gypsum were identified in almost all samples as secondary minerals. Magnesium sulfate minerals are common in our samples, identified as epsomite, polyhalite, pentahydrate, sanderite, kainite, and blodite by XRD profiles. Gypsum dominates within the calcium sulfates, together with low abundance of anhydrite and glauberite. Gordonite, identified in sample F, is also associated to aqueous environments and can be derived during weathering from illite, which was also detected in sample D.

3.2.3. Thermogravimetric Analysis

Thermogravimetric (TG) analysis of three pure gypsum samples was performed on a Thermogravimetric Analyzer Netzsch Sta 409 Pc. in order to determine the molecular weight of water in the crystals before and after dehydration. The purpose of the TG study was to compare the release profiles of three pure gypsum samples from different locations. The samples were hand-picked; sample 1 from the lower part of a yardang (38.09°N, 91.75°E, elevation of 2769 m), sample 2 from the mountain area (38.11°N, 91.05°E, elevation of 3075 m), and sample 3 from the dry playa of Nanyi Mountain (38.06°N, 91.83°E, elevation of 2823 m). Air and nitrogen were used as dynamic atmospheres, with flow rates of 20 $cm^3\ min^{-1}$ for air and 50 $cm^3\ min^{-1}$ for nitrogen.

Figure 5 shows the TG analysis profile for the dehydration of gypsum using a heating rate of 10°C/min. The mass loss observed (solid lines) for the three samples between 80°C and 200°C is due to the loss of the hydrated water of the calcium sulfate [*Van der et al.*, 1999]. The differential scanning calorimetry (DSC) curves (dotted lines) indicate where water was lost. The measured magnitude of water loss was found to be 20% of the original weight, which is in good agreement with the theoretical value of water loss of gypsum [*Van der et al.*, 1999]. The water content (20%) is assigned to water trapped in the gypsum crystals, which is of great importance to the gypsum deposits found on Mars. More facts would need to be collected in further studies in order to see whether it would be feasible to reuse the water contained in the gypsum crystals on Mars.

4. Geomorphologies

A wide diversity of geomorphologic features formed by occasional water, strong winds, and tectonism are well preserved in the Qaidam Basin. The following section is divided in fluvial/aeolian features and tectonic features. An overall description of each of them and our suggested counterparts on Mars are discussed for each of the features.

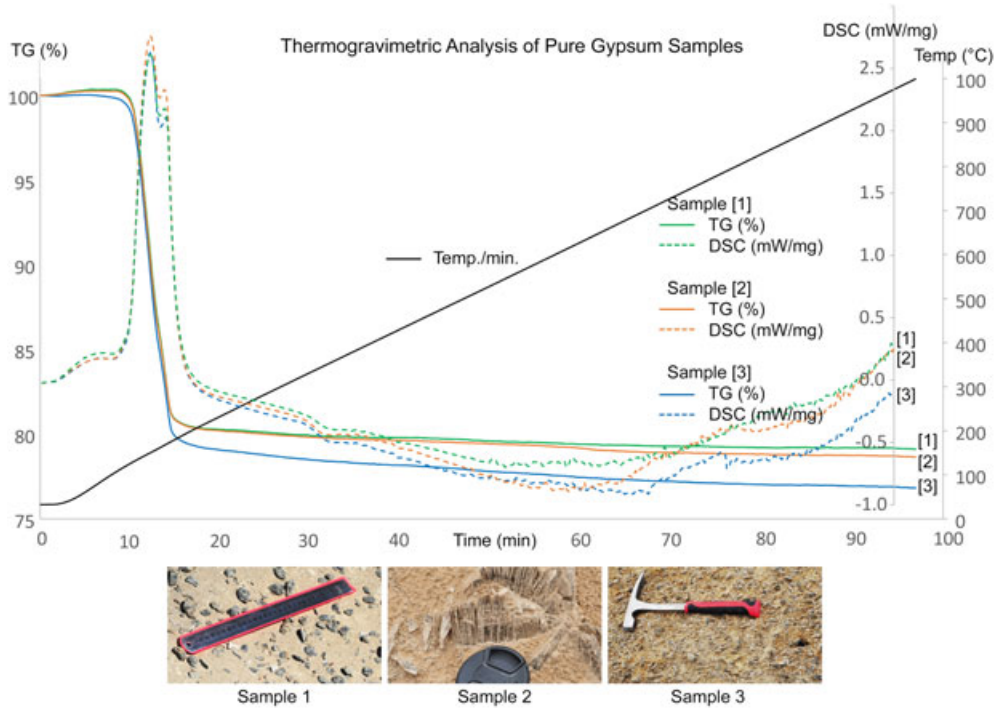

Figure 5. Thermogravimetric analysis. TG and DSC curves for three pure gypsum samples using a heating rate of 10°C/min. The ruler in the picture for sample 1 is 30 cm long. Sample 2 shows a booklet structure of gypsum crystals.

4.1. Fluvial/Aeolian Features

4.1.1. Catastrophic Debris Flows

Structures that appear to be related to catastrophic flow-related processes are retained in the Qaidam Basin. Figure 6a displays what seem to be two different stages in a catastrophic debris flow event that originate from two sources at a very steep area, where the direction of a massive flow is abruptly cut by another flow advancing downslope (the remained part is about 3 km long and 2 km wide). This event might indicate the possible thawing of ice from the upper parts of the mountains in a short time due probably to a sudden warming. An explanation for the 90° change of direction of one of the flows can be understood in terms of the dynamics of compressional flows affected by steep slopes, which causes high velocity of debris and therefore is much more dominant than the adjacent flow that travels westward. Muddy deposits together with water probably weakened and altered the adjacent flow, changing its direction drastically. Figure 6b displays how part of the original debris flow is severely redirected. Figure 6c shows how the redirection only occurs to part of the original debris flow, suggesting that the debris flows occurred as one single event but at two different stages. The redirected terrain forms a massive slope pointing downward to south-southeast (15.5 km long and 2.2 km wide, over a slope with 65 m height difference from the highest to lowest point). The gradual stop of the flow was probably related with the decrease of the slope or/and even by the loss of water by evaporation. The transverse ridges that appear in the lower part of the debris flow (see Figure 6a) suggest that these features transported large amount of sediments that were deposited in the less steep areas. The debris bands result from the extensional flow when the deposits cannot reach the bottom of the slope. Mass flow events of such magnitude are rare on Earth. This process would have a different effect on Mars due to the lower atmospheric pressure and the amount of water required to form such flows; however, Mars exhibits multiple indications of catastrophic mass flows [*Malin and Edgett*, 2000a; *Costard et al.*, 2002; *Mangold et al.*, 2003], especially at high altitudes [*Kargel*, 2004], although there is still some debate on how they formed and continue to form. A discharge of saline groundwater [*Hoffman et al.*, 2000], warmer climatic conditions [*Costard et al.*, 2002], or the melting of water-rich snowpacks [*Christensen*, 2003; *Hartmann et al.*, 2003] are some hypotheses to explain the formation of Martian flows. The majority of flow directions indicate large-scale flows that move downward longitudinally through valleys [*Cabrol and Grin*, 2010]. For example, flow lines in Candor Chasma (Figure 6d) indicate that the accumulation occurs at the valley walls and

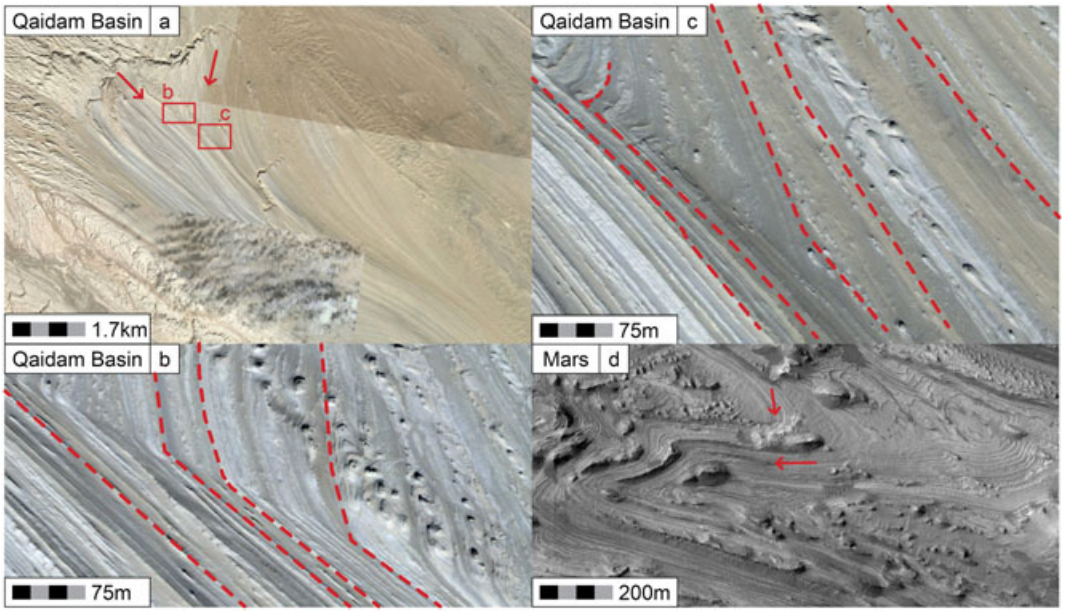

Figure 6. Catastrophic debris flows. (a) Catastrophic debris flow at 38.08°N, 91.88°E in the Qaidam Basin. The altitude is 3077 m. (b) Subframe of Figure 7a showing the change of direction of the debris flow. Note the yardangs that appeared after the debris flow. (c) Subframe of Figure 7a displaying that the original debris flow was only redirected partially, confirming that the flow was one single event but at two different episodes. (d) MOC image showing catastrophic aqueous and sediment flooding in southwestern Candor Chasma, Mars, near 6.6°S, 70.9°W [NASA/JPL/Malin Space Science System].

further flows commonly truncate them [*Kargel*, 2004]. In the Qaidam Basin and on Mars, although there is not a continuous water cycle, the ephemeral water episodes compel the newer flows to adjust to the current conditions; young features display clear signs of ductile flows over former brittle material deformations. This gigantic debris flow in the Qaidam Basin offers a great opportunity to dissect catastrophic debris flows on Mars. Since most hypotheses on the debris flows on Mars assume water-related flows, the study of flow rate and water volume are critical to model and test the previously proposed hypothesis. Further studies of the enormous debris flows in the Qaidam Basin could provide a quantitative estimation of these values based on the slope, mineralogy, and geomorphic appearance of the Martian debris flows.

4.1.2. Polygonal Terrains

Polygonal desiccation terrains are common in the dry playas of the Qaidam Basin. The formation and developing of polygonal terrains are interpreted to be related to freeze-thaw-driven processes of soils containing ephemeral brines [*Lowestein and Hardie*, 1985]. This process is unique of hyperarid environments when a limited input of water enters the system and consequently generates surface or groundwater inflow. The water tends to approach the surface as soon as the surface is leveled and as a result evaporation increases due to the higher concentration of water [*Houston*, 2006]. With an increase of the water evaporation, concentration of salts occurs; hence, the growth of salt crystals in the Qaidam Basin polygonal terrains is only sustained by very scarce quantities of brine ($>$3000 mm of annual evaporation and $<$14 mm of annual precipitation). Rehydration and enlargement occur annually and after hundreds of years the cracks, or inlet channels that delimit the polygons, are well defined [*Thomas*, 2011], as we observed in the remote sensing images and during the field investigations of the Qaidam Basin.

According to their sizes, we observed three distinct types of polygons. The small-sized polygons are commonly a few centimeter in diameter, which probably represent small channels of ephemeral water flows (Figure 7a). Middle-sized polygons are arranged in triangular, rectangular, or pentagonal shapes ranging from 1 to 20 m across, although their size and distribution vary according to local topography (Figure 7b). These middle-sized polygons are all comprised in larger-sized polygon networks, ranging between 100 and 200 m across that contain the smaller polygons within (Figure 7c). The large-sized polygons tend to appear only in the outer edges of the playas. Previous studies suggest that the formation of such large polygons (ranging a few hundred meters in diameter) is created by periods of intense evaporation [*El et al.*, 2012].

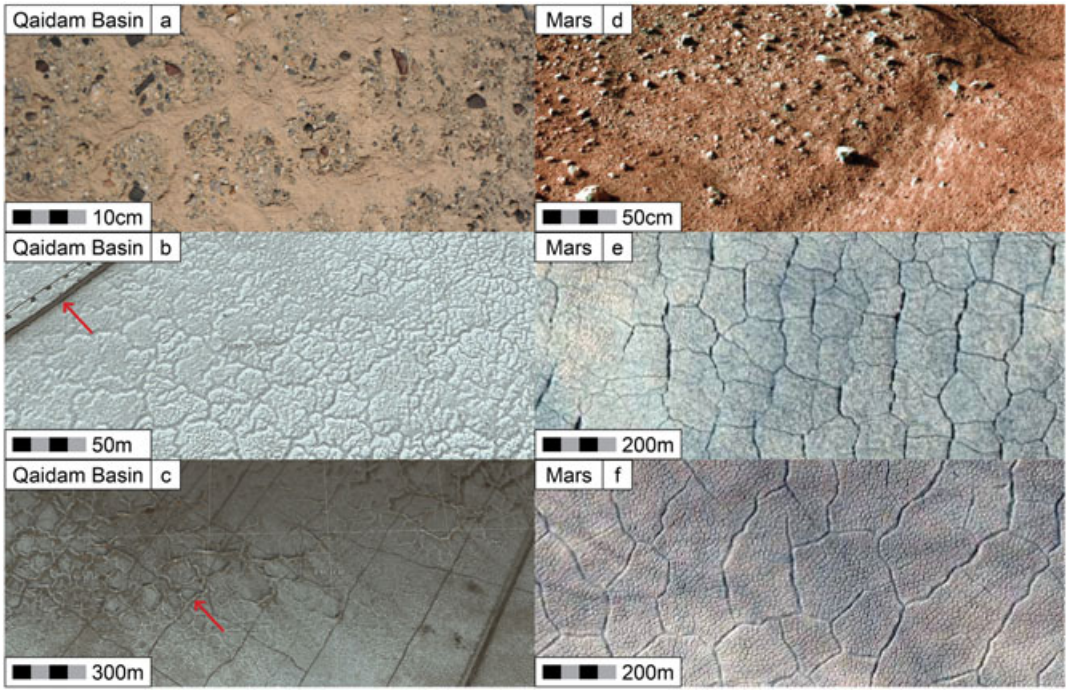

Figure 7. Polygonal terrains. (a) Terrain covered by small-sized polygonal patterns composed of clays with sizes ranging from few milimeters to a few centimeters in the Qaidam Basin. Note the distribution of small rounded pebbles in the polygons, indicating that this area was likely eroded by thaw of ice. (b) Soil polygonally cracked at 38.73°N, 91.64°E. The middle-sized polygonal-patterned saline ground appears with distinctive concentric patterns of a few meters in diameter. The altitude is 2711 m. The red arrow which indicates the thick black line and dashed line in the top left part are a highway and an oil pipe, respectively. (c) Large-sized polygonal saline soils forming networks that were created by centuries of freeze-thaw cycles at 38.75°N,91.75°E. The altitude is 2746 m. The red arrow points a square network made by truck tyre tracks. (d) Image taken by Phoenix's Surface Stereo Imager at the Phoenix Mars lander near 125.74°W, 68.21°N. The small-sized polygonal terrain is composed of fine-grained clays [NASA/JPL-Caltech/University of Arizona]. (e) Middle-sized polygons in Utopia Planitia near 46.7°N, 117.5°E [NASA/JPL/University of Arizona]. (f) Large-scale polygons in Degraded Crater near 62.61°S, 78.77°E [NASA/JPL/University of Arizona].

The middle-sized polygons differ from the other ones in their elevated and fractured center, where vents and pores suggest the presence of subsurface depressions or voids (see the polygon center in Figure 9). Inside these voids we could observe stalactite-like halite crystals of a few centimeter in size.

Similar-sized polygons on Mars are shown in Figure 7d (small-sized), Figure 7e (middle-sized), and Figure 7f (large-sized). The formation of polygonal patterns on Mars has been recently proposed to be related to ephemeral lakes that probably underwent repeated cycles of desiccation and recharging by ephemeral surface or near-surface water [*El et al.*, 2010, 2013]; thus, the salt-rich playas of the Qaidam Basin are good potential analogues for such features. The polygonal terrains of the Qaidam Basin could be further investigated and used as stratigraphical and paleoenvironmental indicators to investigate the thickness and composition of the Martian polygonal terrains.

To confirm the presence of brines in the polygon cracks, we analyzed two samples from a polygonal structure in the Qaidam Basin: one sample from the polygonal crack and another sample from the polygon center (Figure 8). Our XRD peak positions display sharp peaks and little background absorption. The mineralogy of the sample in the center of the polygon can be attributed to an assemblage of gypsum, quartz, and halite; while the mineral assemblage in the polygonal crack is assigned mainly to halite, clinochlore, epsomite, and pentahydrate, all related to the hydration and evaporation of water. The spectra display characteristic sulfate minerals and indicate the presence of evaporites. The minor shifts in some XRD peaks (not shown) may be due to the presence of natural impurities on the crystal structures. The analysis confirms the presence of salt crystals in the polygonal cracks despite the limited water activity in the Qaidam Basin. Ephemeral water episodes and minimal melting indicate that there are particular processes in developing these polygons in extreme conditions and bears critical information on the similar processes observed on the Martian surface.

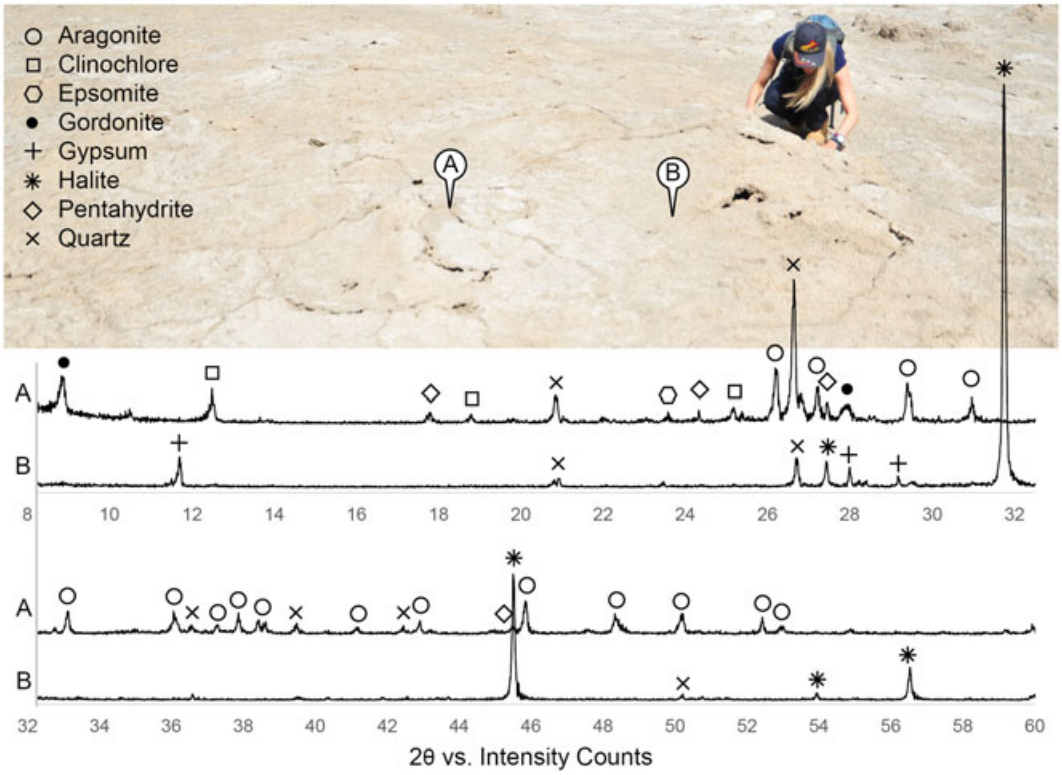

Figure 8. The mineralogy of Polygonal materials. X-ray diffraction of the bulk materials from a polygon crack (A) and polygon center (B) samples in the western Qaidam Basin at approximately 38.46°N, 91.21°E. The peaks imply the presence of brines.

4.1.3. Hollows and Pits

Mountain crests in the Qaidam Basin record a variety of unique geomorphic structures characterized by relic pit-like forms and hollows ranging in size from a few meters to a few kilometer across (Figure 9a). Such patterns appear only in flat and high-altitude areas, in contrast to lower areas that do not display such modification of the surface of the underlying sedimentary material. Most of the pits look empty, and they are not filled with any material. Some of them are interconnected and form larger depressions, whereas others may have smaller pits within (Figure 9b). The edges look generally irregular and sharp, with an outward extending wall where the rocks seem to be rough. Some of the pits are tear-like, showing a preferred direction from the top left to the bottom right of the figure. We suggest that these geomorphic structures seem to be formed by a range of processes and environmental conditions suggesting sandblasting and eolian erosion, together with a possible accumulation of ice that lead to the formation of irregular depressions. For this to occur, the only probable source of water had to be originated in the upper mountain areas, where ephemeral accumulated ice appears at an altitude of ~3300 m. Figure 9c shows the upper mountain areas with accumulated ice. We suggest that accumulated ice stores fill the depressions and are later removed by sublimation or by interconnected flows of mixed thawed ice and clay materials, which may vary according to flow density, temperature, and downslope motion processes (see Figure 9a).

Consistent with this interpretation are a series of hollows observed in the upper mountain crests (about 5000 m high) in the center of Gale crater (Figure 9d). Some of the pits display steep walls and sharp divides between them [*Fairén et al.*, 2014]. *Anderson and Bell* [2010] describe these features as "alcoves." This topography has been attributed to glacial foregrounds, where buried ice melts out to create the hollows or depressions [*Evans and Twigg*, 2002]. The pits look like empty spheres or ellipsoids, although some are much more irregular in shape. The pits are filled with relatively bright soil material. *Fairén et al.* [2014] suggest that all the morphologies of Gale crater correspond to late-stage water and/or ice activity. The last occurrence of ice near the equatorial region was suggested to happen as recent as the Late Amazonian epoch [*Dickson et al.*, 2008], but these migrations of ice toward the equator would not have involved the presence of

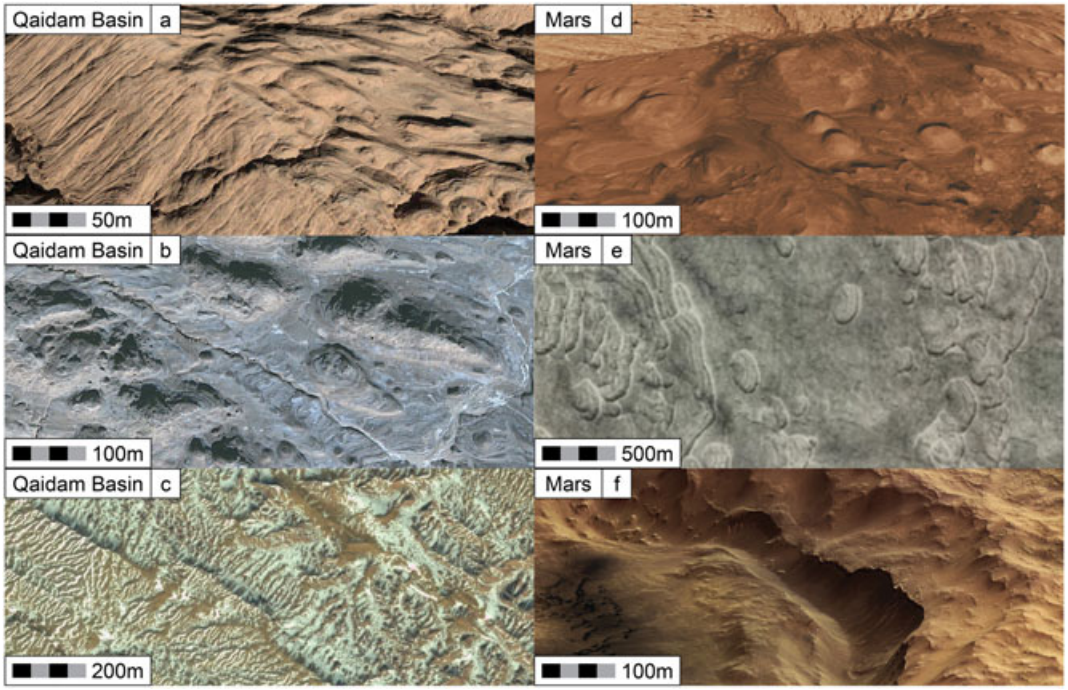

Figure 9. Morphologies produced by possible episodic accumulation of ice on high-altitude areas. (a) Rounded pits located in the plateau area in the Qaidam Basin at a location near 38.67°N, 91.17°E. The altitude is 2924 m. (b) Hollows appear distributed on the mountain area at 38.32°N, 91.2°E. The altitude is 2873 m. (c) Ephemeral snow captured by satellite image of the mountain crests in the Qaidam Basin near 37.64°N, 94.99°E at 3323 m. (d) Irregular pits in the mountain crest in the center of Gale crater on Mars near 5.4°S, 137.8°E [NASA/JPL-Caltech/ESA/US]. (e) MOC image M0203335. Scalloped topography is characteristic in the Utopia basin at approximately 46.9°N, 117.36°E, where hollows seem to have formed by the sublimation of the ice-rich permafrost [NASA/JPL/Malin Space Science System]. (f) Rounded mounds on top of Maunder crater on Mars near 50°S, 358.5°W, in the center of Noachis Terra [ESA/DLR/FU Berlin].

liquid water [*Head et al.*, 2003] and so could not have formed the features of Gale crater [*Fairén et al.*, 2014]. The morphologies provide information of the last time when ice was present and was enough to modify the lithology [*Fairén et al.*, 2014]. Figure 9e displays scalloped topography in Utopia Basin, where uneven depressions may be indicators of the presence of ice-rich sediments and ground ice, where pits are combined with polygonal fracturing [*Carr*, 2006]. Some of the pits are shallow and others seem deep, planimetrically irregular and show no preferred orientation. These hollows and polygons were suggested [*Carr*, 2006] to be outcomes of the removal or redistribution of surface ice and groundwater during warmer periods. Figure 9f displays another example of an upper alcove with disrupted topography and irregular mounds in Maunder crater, located in the southern midlatitudes of Mars. The upper altitude surface looks like a combination of pits that are separated by small knobs or ridges of different prominence. The numerous knobs combined with the depressions complicate the surface. There is no preferable orientation of these pits; some are very deep and less defined. This is obvious not only from the satellite image but also from the fact that there are shadows inside them. According to *Head et al.* [2005], the deposits on Maunder crater are lines of evidence for recent glacial activity during epochs of increased obliquity that promote the accumulation of ice and snow in tropical and midlatitude regions. Bed sliding structures appear also in the walls of the crater that can be explained by hydrodynamic processes [*Malin and Edgett*, 2000a], verifying the scale of water redistribution and volumes of buried ice in the Martian midlatitudes [*Head et al.*, 2005].

The observed pitting in the Figures 9a and 9b, in their most developed form, produces delicate surface textures. It is unlikely that they formed by a catrastrophic mass flows. So these features are either predepositional or postdepositional of mass/ice flows. Based on analogy with the Qaidam Basin, the pits in Gale crater, Utopia Basin, and Maunder crater might be the result of the accumulation of ice during high obliquities, although wind activity may play a role too. An analysis of the pit morphology, size, and distribution is

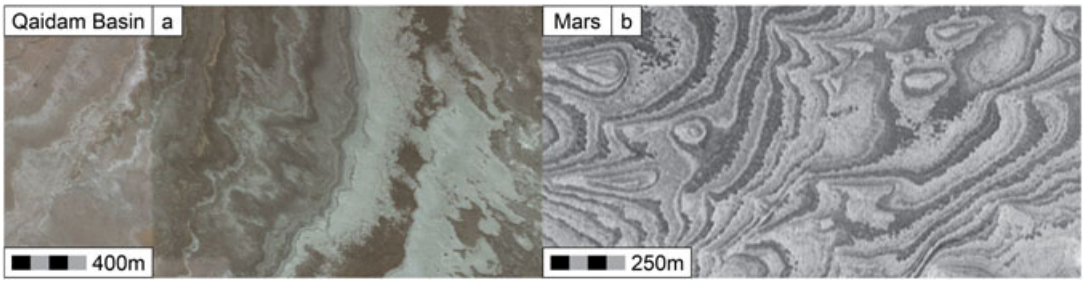

Figure 10. Cyclic vertical accretion. (a) Depositional features mark the lake layers, showing evidence for vertical accretion at 38.75°N, 91.74°E. The flow features display dark patches, occurring on outer layers of the playa and associated with lighter material. The altitude is 2750 m. (b) MOC image R1800383 of cyclic vertical accretion on Becquerel crater near 21.1°S, 8.5°E [NASA/JPL/Malin Space Science System].

necessary in future studies of the Qaidam Basin. If the pits are the product of accumulation of water/ice and eolian processes, the different density of pits means that the times of rock exposure to accumulate water/ice were different or the susceptibility of lithologies to be pitted by the action of winds varies significantly, according to differences in lithology or composition, or both. Further study is needed to support or refute a water/ice accumulation hypothesis to explain these features. According to *Fairén et al.* [2014], there is no known nonvegetation terrestrial analog that can be compared with the Gale; thus, the Qaidam Basin can be a good potential analog to recreate the pits and hollows in the equatorial regions of Mars. Understanding the details of processes that carved hollows and pits demands further study.

4.1.4. Cyclic Vertical Accretion

The playas of Xiaoliang, Nanyi, and Jianding Mountains are tectonic anticlines [*Anglés and Li*, 2016] that display alternate layers of salts and clays that can reach several hundred of meters wide in steeper areas (Figure 10a). The layered features in Figure 10a belong to the dry playa of Dalangtan, in the most northern part of the Qaidam Basin. The Quaternary evaporite sediments display features such as vertical accretion or lamination plastered on a preexisting slope. These sedimentary deposits have been associated to the lake shorelines or receding floods of the ancient lake, when the precipitation of salts occurred [*Zheng et al.*, 1993; *Zheng*, 1997]. The complexity of some facies patterns suggests that their formation was influenced by multiple factors, for example, brine concentration and evaporation over long periods of time, aeolian effects, local steepness, and deposition under different climatic conditions over long time scales.

The presence of dry lakes on Mars has been confirmed by a number of missions, both from surface and by orbital means [e.g., *Cabrol and Grin*, 2010; *De Hon*, 1992; *Forsythe and Blackwelder*, 1998; *Irwin et al.*, 2005]. One example is the layers of evaporites and clays in the deposits of Becquerel crater (Figure 10b), where the low-albedo layers have been associated with high levels of hydrated minerals such as sulfates and halides [*Grotzinger and Milliken*, 2012]. The presence of layers is consistent with successions related to climate change and brine cycling [*Grotzinger and Milliken*, 2012]. High Resolution Imaging Science Experiment (HiRISE) determined layers up to 36 m in thickness, most of them parallel to each other indicating that they formed by vertical setting produced by the effects of water [*Carr*, 2006]. The different layers appear to be easily eroded by aeolian effects, even in their current conditions [*Grotzinger and Milliken*, 2012]. While mineralogical and morphological evidence of layering in dry playas on Mars is clear, the stratigraphic successions are still under debate and lack a precise link of these features to ancient lakes [*Cabrol and Grin*, 2010]. Cyclic vertical accretion structures in the Qaidam Basin might be able to give some hints to this question in further studies.

4.1.5. Recurring Slope Lineae

The HiRISE instrument identified in the midlatitudes of Mars unique structures that are characterized by their low contrast albedo, their preference in equatorial slopes, and their appearance mainly during spring and summer, termed Recurring Slope Lineae (RSL) [*McEwen et al.*, 2011]. Recent literature suggest that the RSL on Mars might be due to the intermittent flow of briny water [*Chevrier and Rivera-Valentin*, 2012; *McEwen et al.*, 2014; *Ojha et al.*, 2015]. An alternative hypothesis suggests that they could form from deliquescence and is later trapped by hygroscopic salts [*Levy*, 2012; *Dickson et al.*, 2013], however it is still not clear if the Martian atmosphere could supply enough water vapor to create those features [*McEwen et al.*, 2014]. RSL are active features on Mars today, but their origin still remains an open question.

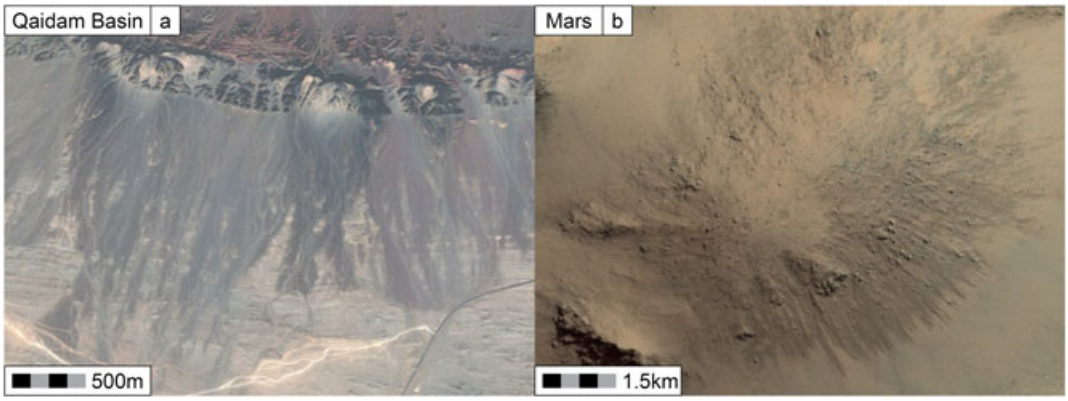

Figure 11. Recurring Slope Lineae. (a) Dark streaks appear in a 80 m high slope at a location near 41.68°N, 91.87°E. The altitude is 1224 m. (b) Subframe of a HiRISE image PSP_005787_1475 located near 32.04°S, 140.80°E. The image shows RSL in an uplift of an unnamed crater on Mars [NASA/JPL/University of Arizona].

Streams of small scale flow features of low reflectance in comparison to the surrounding terrain appear in some slopes in the Qaidam Basin. They are similar in planform morphology to those low albedo streaks identified on Mars. Figure 11a displays a good example of groundwater sapping features that resemble the RSL on Mars (Figure 11b). It is known that the RSL on Mars advance and recede each year, starting again when the surface temperatures are close to the melting point of water [*McEwen et al.*, 2011]. The McMurdo dry valleys in Antarctica have been previously proposed to be the closest analog for RSL on Earth, where deliquescences together with small amounts of meltwater are able to produce brines that mimic the RSL formation on Mars [*Dickson et al.*, 2013]. We have evidence of seasonal brines in the Qaidam Basin [*Kong et al.*, 2013]; thus, the identification of such features warrants a further characterization and analysis, as they may provide new clues to their origin on Mars.

4.1.6. Gullies

Occasional gullies appear in the mountain areas in the Qaidam Basin. They can be hundreds of meters long and follow the local topography as they descend (Figure 12a). They normally form on hillsides after

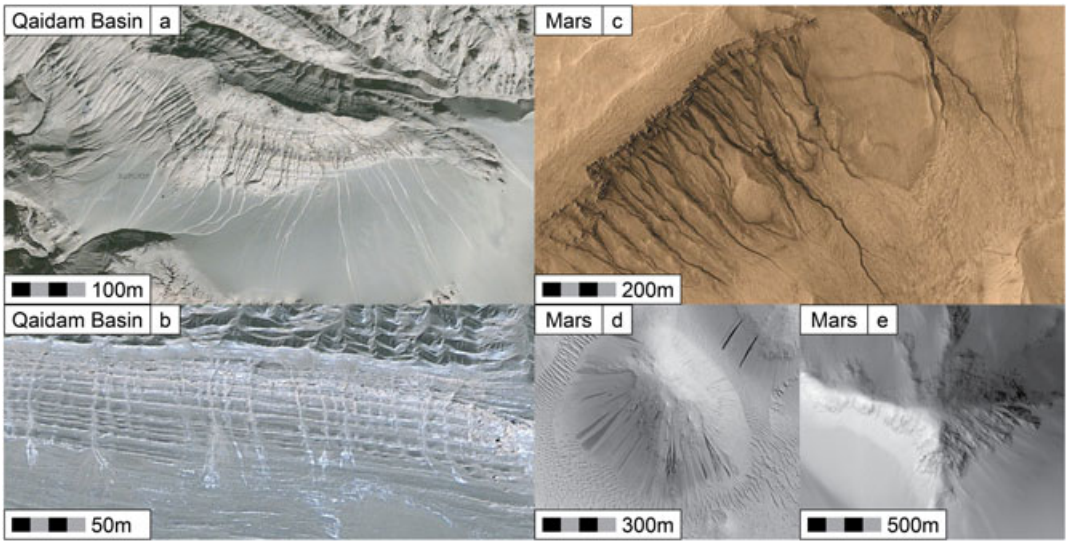

Figure 12. Gullies. (a) The valley shows evidence of fluvial erosion in the Qaidam Basin at 38.32°N, 91.27°E. The altitude is 3374 m. (b) The color of the gullies stream is white, indicating high salt concentration. Image at 38.32°N, 91.27°E. The altitude is 2876 m. (c) High-resolution image of gullies on Newton Basin near 40.8°S, 201.9°E, taken by Mars Global Surveyor robot spacecraft [NASA/JPL/Malin Space Science Systems]. (d) MOC image MOC21621-d of dark slope streaks around obstacles in the Aeolis region of Mars at 1.5°S, 202.9°W [NASA/JPL/Malin Space Science Systems]. (e) Activity is highly concentrated in the southern walls of the heavily eroded hill in the southern part of Juventae Chasma at 4.7°S, 298.6°E [NASA/JPL/University of Arizona].

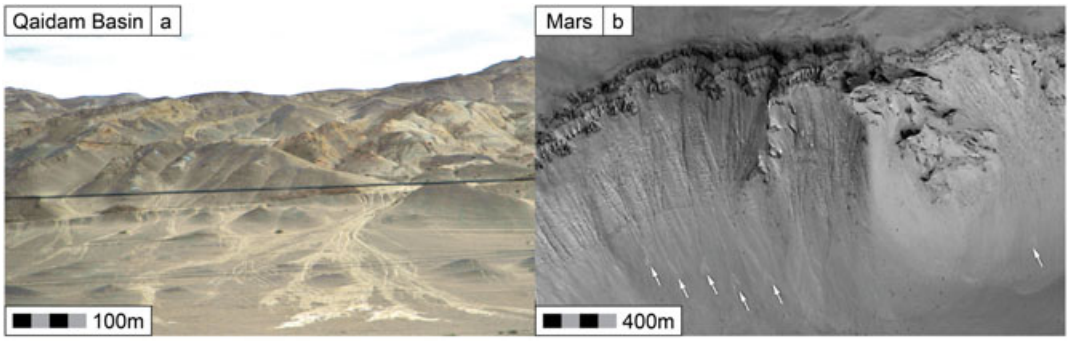

Figure 13. Light-toned gullies. (a) white gullies in the Qaidam Basin near 38.58°N, 95.14°E at about 3398 m altitude. (b) The arrows point white materials in the gullies of Noachis Terra near 47.2°S, 355.8°W on Mars. The image is a mosaic of MOC images M11-00286, S13-01274, and R09-01804 [NASA/JPL/Malin Space Science Systems].

ephemeral rain episodes; however, water flow could also emanate from the melting of accumulated ground ice on top of the plateau. The ridges, however, are not able to sustain high amounts of groundwater due to their limited area and the strong evaporation that characterizes the Qaidam Basin. A suggestion is that an ice cap was stable for a period of time and episodically melted, providing the limited amount of water that was episodically flowed under a very strong evaporite condition. The strong evaporation levels and limited precipitation imply that the occurrence of salts interacting with thawing ice or water is limited, as new gullies are rarely seen following the line of former gullies (Figure 12c).

On Mars, the main difference between gullies and RSL is that gullies have been found to take place mainly during winter and do not have an albedo contrast [*Dundas et al.*, 2010; *Diniega et al.*, 2010; *Dundas et al.*, 2012]. Despite the main period of outflow channel formation ended by the late Hesperian [*Cabrol and Grin*, 2010] and the current low temperatures, gullies have been detected in many locations [*Malin and Edgett*, 2000a, 2001; *Balme et al.*, 2006]. A plausible interpretation is that those Martian gullies result from the temporary melting of former ice caps and snow at the higher latitudes during high obliquities [*Christensen*, 2003; *Costard et al.*, 2002; *Lee et al.*, 2001]. In the presence of salts, small amounts of liquid water might be stable under current Martian conditions causing gullies to form on the slopes of hills [*Malin and Edgett*, 2000b]. The findings reported in the last decades request to narrow the theories about the mechanisms behind the gullies' formation on Mars. Gullies of a few meters across appear for instance on the slopes of Newton crater (Figure 12c), Aeolis region (Figure 12c), or in Juventae Chasma (Figure 12c).

We observed in the gullies of the Qaidam Basin that water transports fine clay particles creating smooth surfaces that are reflected in the satellite images as high albedo zones (Figure 13a), contrary to those areas away from the gullies where the relatively dark color is made by the cover of coarse grains on the surface. Similar high-albedo gullies on Mars are shown in Figure 13b. Figure 14 displays the XRD patterns obtained from the high-albedo material of a gully sample. The peaks are sharp with little background absorption. The crystal structure of the minerals confirms the presence of halite, quartz, and calcite as major minerals. The extra reflections are due to the presence of anhydrite, clinochlore, pentahydrate, and polyhalite.

Gullies are widely distributed in the Qaidam Basin in association with polygon-patterned soils (Figure 15a), strongly indicating that some temporal relationships within the polygons and gullies might occur. Polygonal grounds appear on the fans annexed to the slopes containing gullies; hence, the gullies may play a role in the transport and accumulation of snow and melted water. The ephemeral water from the gullies is probably accumulated in the fans near the slopes, and after years of freeze-thaw-driven processes due to the strong evaporation of the area, the hydration and rehydration of the existing salts form the observed polygonal patterns. Similar relationships (Figure 15b) have been identified between gullies and patterned terrains on Mars [*Levy et al.*, 2009a]. The HiRISE instrument provides a unique view of the detailed relationships of gullies and thermal contraction cracked polygons over a wide range of zonal climatic conditions [*Levy et al.*, 2009a], and as it happens in the Qaidam Basin, they normally form in the sediments layer on terrains adjacent to gully structures [*Christensen*, 2003; *Costard et al.*, 2002]. A few studies already considered the interactions between gullies and thermal contraction crack polygons on Mars (termed "gulligons') [*Levy et al.*, 2009a, 2009b, 2009c, 2011]; however, the similarities that the Qaidam Basin offers with the Martian gullies and their

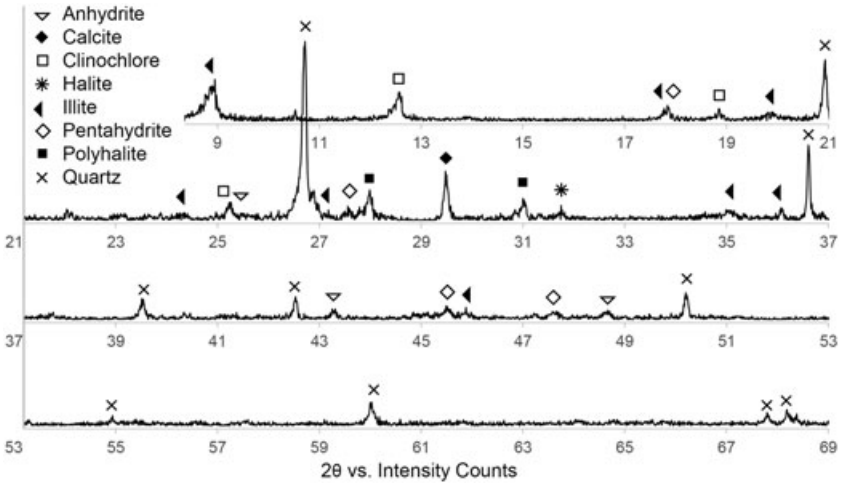

Figure 14. The XRD measurements of gully materials. The occurrence of the main peaks of each mineral is represented in the XRD spectra of a gully sample.

related well-developed crack polygons could provide key information to interpret the permafrost development of Martian soils.

4.1.7. Fluvial Valleys and Alluvial Fans

The development and distribution of fluvial valleys, alluvial fans, and playas depend largely on the local hydrologic conditions. Fluvial valleys in the Qaidam Basin are broadly distributed. Most of them are found in the surrounding mountains of the basin and are formed by occasional rainfall and ice thaw [*Kong et al.*, 2014]. Runoff from the large mountainous catchment transports large amounts of clastic material and dissolved ions to the basin [*Yu et al.*, 2013]. For example, the Dalangtan playa was formed in the syncline depression surrounded by rock hills of Neogene strata [*Yu et al.*, 2013]. The playa received surface runoff from alluvial fans that were formed along the piedmont of the Altun-Tagh Mountain [*Yu et al.*, 2013]. The

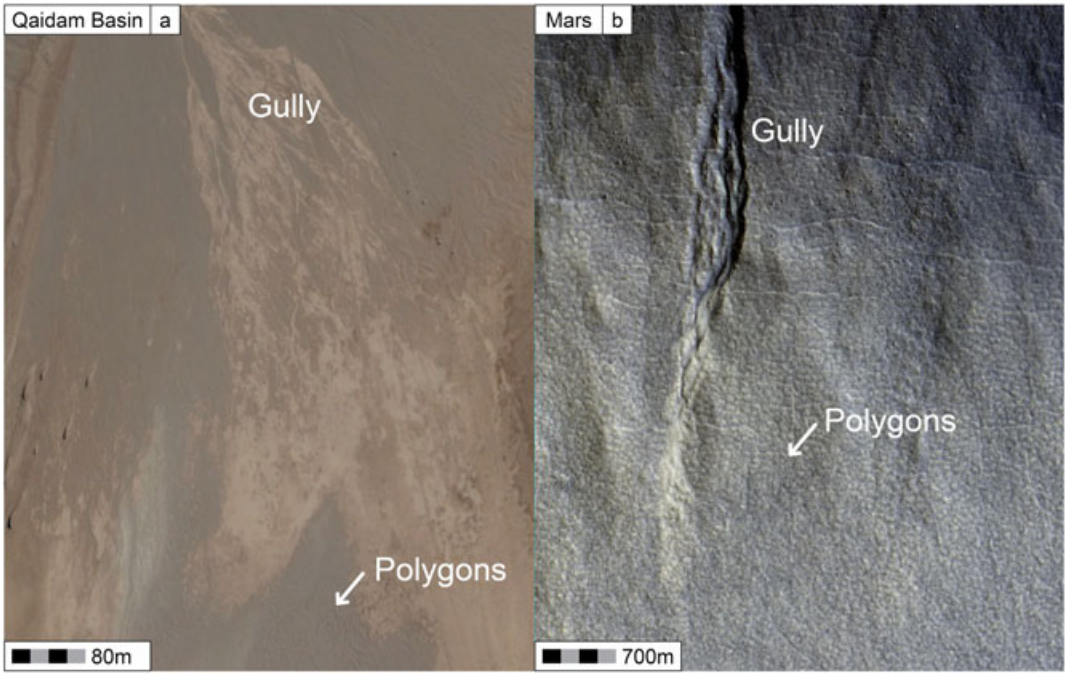

Figure 15. Gullies in association with polygons. (a) Polygonal soils appear on the slopes containing gullies at 38.57°N, 91.95°E in the Qaidam Basin. The altitude is 2731 m. (b) HiRISE image PSP_001846_2390 located at 58.74°N, 82.38°E of polygons present on gully fans [NASA/JPL/University of Arizona].

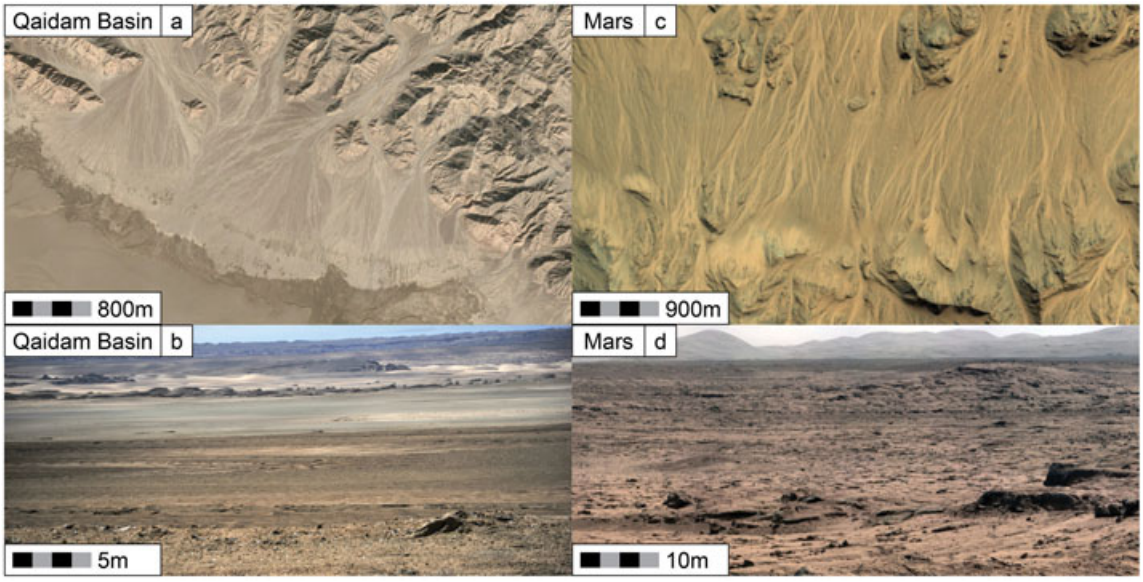

Figure 16. Fluvial valleys and alluvial fans. (a) The alluvial fans in the Qaidam Basin are compelling evidence of continued water erosion and subsequent deposition at 39.16°N, 92°E. The altitude is 2826 m. (b) Large alluvial fan in western Qaidam Basin near 39.16°N, 92°E. (c) Fans in the Mojave Crater in the Xanthe Terra region of Mars at 7.5°N, 33°W [NASA/JPL/University of Arizona]. (d) The panorama of a large alluvial fan is a mosaic of images taken on the Rocknest location at approximately 4.6°S, 137.43°E by the NASA Mars rover Curiosity [NASA/JPL-Caltech/Malin Space Science Systems]. The scale bars for Figures 16b and 16d are for the nearest place in the bottom of the picture.

fluvial fans in the Qaidam Basin appear with different sinuosities and depths, depending on where they originate. The mountains in the Qaidam Basin have a granitic origin, although small mountains in the southeast of the basin consist of clastic sedimentary rocks, making the fluvial fans deeper and more dispersed. They normally display V-shaped morphologies and can measure hundreds of kilometres long (Figure 16a).

The terminal fans display wide unchanneled flows and are composed of sediments that distinctly end at the dry lake where aeolian erosion assists in leveling the surface. The alluvial fans tend to be large and fan-like, extending for several kilometers with an elevation difference of less than 100 m (Figure 16b), although elongated and lobate distal morphologies were observed too.

On Mars, most fluvial fans are witnessed in the southern highlands, and the majority of them are considered to be formed by liquid water [*Gulick*, 2001; *Howard et al.*, 2005; *Fasset and Head*, 2008]. For instance, the Mojave crater in the Xanthe Terra (Figure 16c) and the Rocknest location (Figure 16d) are examples of extended terminal fans. In the Mojave crater, the lower unit of the crater displays an initial deposition which most probably evolved into an alluvial setting, presupposing limited water activity [*Cabrol and Grin*, 2010]. Polygonal terrains at the terminal fan are also consistent with a considerable decline of water over time [*Cabrol and Grin*, 2010]. The area represents the end of an extended history of aqueous activity and deposition [*Cabrol and Grin*, 2010]. The Mojave crater morphology is similar to many other craters on Mars [*Cabrol and Grin*, 2010], suggesting that similar processes occur all over the planet. However, many factors have to be considered in valleys and alluvial fans formation; hydrologic, climatic, lithologic, and tectonic factors control fan development [*Moore and Howard*, 2005]. The link between alluvial fans and climatic conditions can be much more complicated than previously indicated for the alluvial fans on Mars [*Cabrol and Grin*, 2001]. They stated that elongated fans are formed on Mars during high-discharge periods, whereas fan-like and lobate deltas are indicators of arid periods and tend to occur in small basins. The alluvial fans in the Qaidam Basin are elongated, fan-like, lobated fans formed by mudflows or by fluvial deposition, but they were all formed within the same enormous basin that underwent varied climatic conditions. The different shapes in the fans might be related to other factors that affect the morphology. The complex interaction of deposition and erosion, which is diagnostic of fan evolution on Mars, cannot be studied exclusively from orbital data. It is understood that particle sizes, surface gravity, fan geometries, or flow properties are different on Mars; however, a deeper investigation of the scaling relationships among the valley networks and alluvial

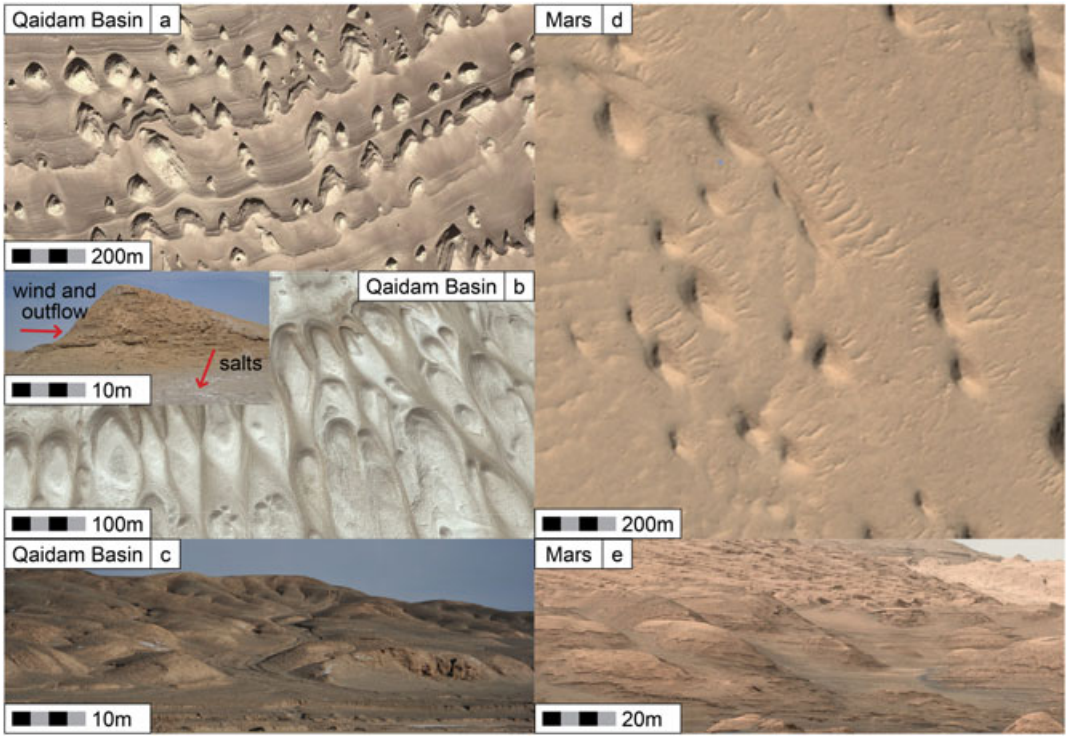

Figure 17. Yardangs. (a) Features of erosional progression of the serrated facies of yardangs in the valleys of Nanyi Mountain at 37.61°N, 92.23°E. The altitude is 2983 m. (b) Progression of remnant V-shaped yardangs at 37.71°N, 92.58°E. Note the eroded facies and the teardrop-shape. The altitude is 2873 m. (c) Scoured ground and teardrop-shaped islands are very common on the Qaidam Basin. Picture taken approximately at 38.31°N, 90.81°E. (d) Yardangs in Aeolis Planum at 2.83° N, 147.64°E [NASA/JPL/University of Arizona]. (e) This mosaic of images were taken by the Mastcam on NASA's Curiosity Mars rover, where yardangs appear distributed on the lower part of Mount Sharp at 5.08°S, 137.85°E [NASA/JPL-Caltech/MSSS]. The scale bars for Figures 17c and 17e are for the nearest place in the bottom of the picture.

fans on the Qadaim Basin could provide an opportunity to assess the fluvial and eolian processes on the Martian surface.

4.1.8. Yardangs and Wind Streaks

The north-western part of the Qaidam Basin contains one of the highest- and largest-elevation yardang fields on Earth [*Kapp et al.*, 2011; *Li et al.*, 2016; *Rohrmann et al.*, 2013]. In addition, the high altitude and atmospheric pressure of ~709 bar, about one third lower than normal pressure [*F. J. Kong et al.*, 2013], make the wind imprint even more remarkable. Although yardangs are mostly present in desert areas on Earth, they are normally limited in extent and tend to be small [*Laity and Bridges*, 2013]. Eolian erosion and seasonal/ephemeral runoff from the surrounding mountains were the dominant exogenous factors to sculpt the yardangs during the Pleistocene in the Qaidam Basin [*Li et al.*, 2016]. The Holocene was a much drier period in the Qaidam Basin, and as a result, only wind was responsible for carving the yardangs in the basin, except those yardangs near piedmonts that were affected by the limited fluvial erosion from surrounding mountains [*Li et al.*, 2016]. Today, given the current hyperarid conditions in the Qaidam Basin, strong and consistent unidirectional winds are the primary factor contributing to yardang formation and orientation as well as exposing the stratigraphic relationships in the different facies [*Kapp et al.*, 2011].

Although wind plays the main role, many other factors surely influence their formation, including climatic conditions, chemical weathering, mass wasting, sediment characteristics, or intensity of runoff. All these factors have created a wide variety of morphologies in the yardangs. Some of them are explained below.

Li et al. [2016] classify the yardangs in the Qaidam Basin into eight categories. Here we only present cone-shaped yardangs (Figure 17a) and long-ridge yardangs (Figure 17b). The role of strong aeolian erosion in the long-ridge structures is clear on remote sensing images where the geomorphic expression of the yardangs can be clearly recognized by their alignment and linear nature. The long-ridge yardangs are normally

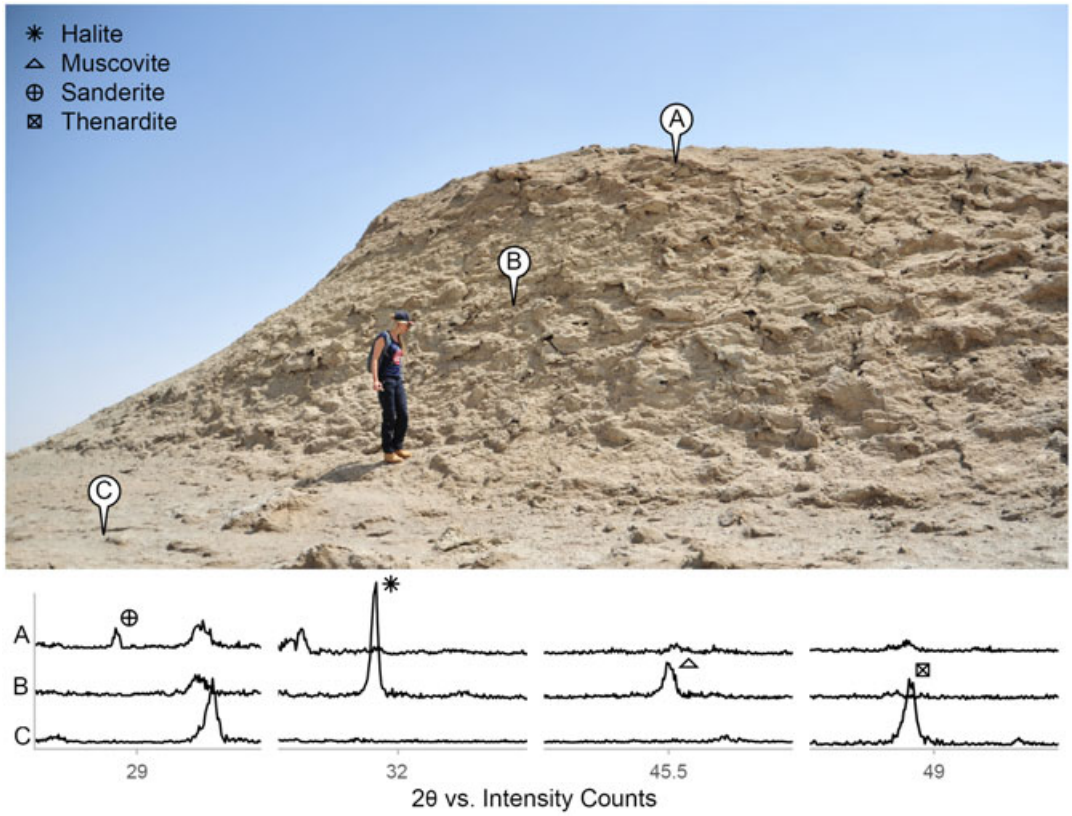

Figure 18. Yardangs analysis. Mineralogical differences detected by XRD analysis between the upper part of a yardang, middle part and lower part.

about 20–50 m high, and they are more common. They are surrounded by small aprons with well-developed flat fronts and steep walls, due to the removal of material and sediment collapse. The cone-shaped yardangs are normally about 10 m high, they form small residual pyramids with a flat or smooth tops (Figures 17a and 17c). These yardargs have been more affected by fluvial erosion and so they have less streamlined morphology and more ambiguous orientations [*Li et al*., 2016].

Mars contains many examples of yardangs, especially in equatorial regions [*Ward*, 1979; *Greeley and Iversen*, 1987; *Mandt et al*., 2008; *De et al*., 2010], although they are relatively less studied compared to other morphologies on Mars. Among the most abundant yardang fields on Mars, the Medusae Fossae Formation, located along the equatorial region, has been termed enigmatic because its origin has been debated for the last decades [*De Silva et al*., 2010]. Other than Australian desert yardangs, very few examples are known on Earth; however, the Australian yardangs are not characterized by extremely low annual precipitation [*Goudie*, 2007]. Despite the fact that Martian yardangs are bigger (approximately 50 km long, 1 km wide, and 200 m high), they were formed relatively recently in the Martian geological history [*Ward*, 1979]. The formation of yardang systems in the Qaidam Basin is recent, and it is characterized by extremely low annual precipitation. In this contribution, the well-observed yardangs in the Qadaim Basin could provide new analogues to a better understanding of the yardang formation on Mars.

To note the similarities, an example of cone-shaped and rounded yardangs appears, for instance in Aeolis Planum (Figure 17d) and in Mount Sharp, where the Curiosity took a close view of rounded yardangs (Figure 17e). The rounded yardangs in Mount Sharp contain sulfate minerals that suggests a possible change in the water availability at the time of their formation [*Wray*, 2013]. Besides water and wind, weathering, desiccation, and mass movements should be used as well as a comparative study to provide insights into yardang formation on Mars.

Our XRD measurements show that the yardang materials are mainly composed of detrital quartz, gypsum, calcite, and clinochlore. Small mineralogical differences exist between the lower parts of the yardangs, the

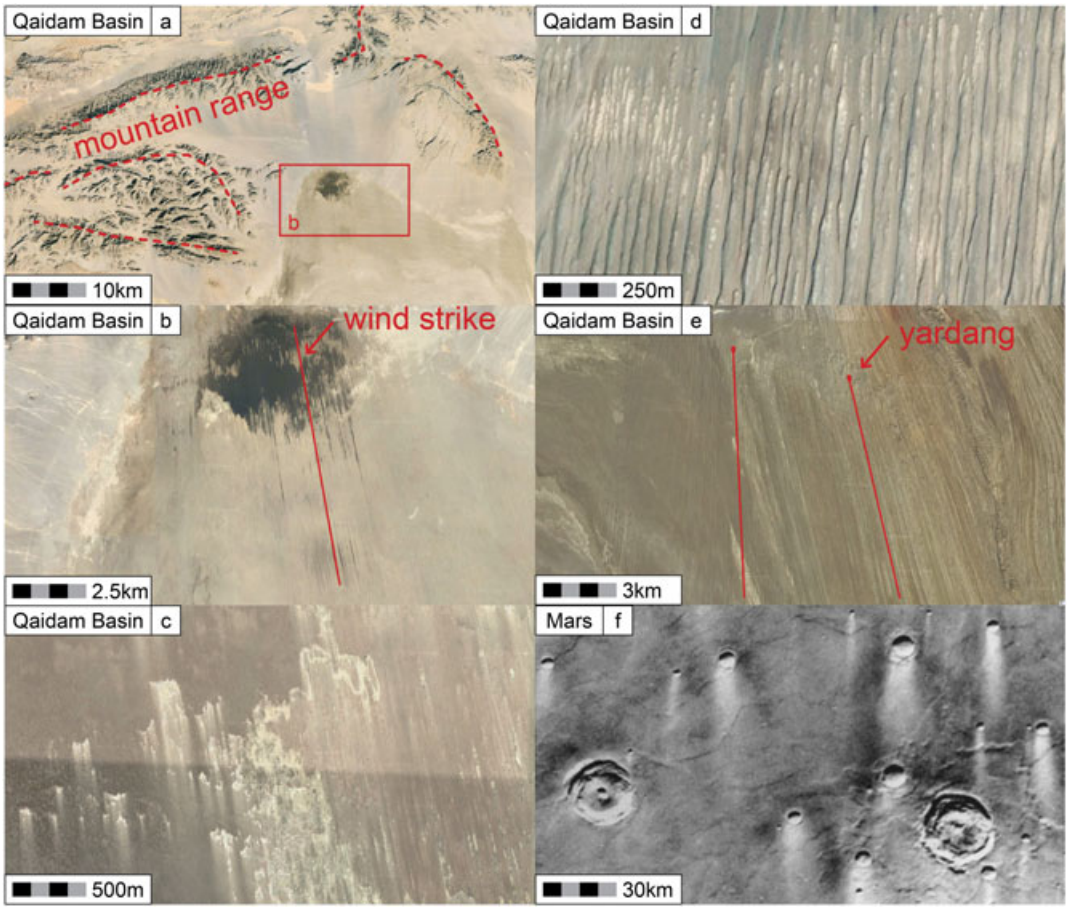

Figure 19. Wind streaks. (a) Source of wind in between mountain ranges in the Qaidam Basin at approximately 38.89°N, 92.29°E. (b) The wind streaks appear at 38.79°N, 92.33°E at 2718 m. (c) Bright wind streaks appear on the surface due to the extremely strong winds at 38.49°N, 92.40°E at 2707 m. (d) The image displays the abundance of thin and elongated yardangs at 38.48°N, 92.28°E at 2727 m. (e) The yardangs can be up to 10 km long at 38.76°N, 92.42°E at 2729 m. (f) Viking Orbiter frame 375S11 of bright wind streaks located at 8.17°N, 297.39°W on Mars [NASA/JPL-Caltech/Malin Space Science Systems].

middle, and the upper parts (Figure 18). Sanderite was detected in the upper part of a yardang, a magnesium sulfate also detected on Mars in the silica-rich deposits and hydrated minerals of Gusev Crater [*Rice et al.*, 2010]. Muscovite was detected in the middle of the yardang, a common detrital mineral associated with quartz. The lower parts display thenardite, an anhydrous sodium sulfate mineral typical of evaporate environments. Thenardite can gradually absorb water and transform to mirabilite ($Na_2SO_4{\cdot}10H_2O$); however, mirabilite was not detected in the yardang samples, confirming the extreme dry environment of the area.

In the northern part of the study site, at approximately 38.54°N, 92.46°E and ~2700 m altitude, the wind imprint is much more remarkable than in other areas of the Qaidam Basin. This is probably due to the width of the valley (~70 km wide) and the shielded area from the three surrounding mountains that probably constrains the strength of the wind (Figure 19a). Here we present an examination of wind streaks that provide evidence of unidirectional and strong winds and localized erosion. Figure 19b displays the area that might be the source of wind, as the surrounding mountain ranges and slopes do not display any aeolian modification. The wind streaks display no topographic relief on their own; the streaks cross the surface without any interruption. The features appear brushed away (Figure 19c) extending for up to ~2 km. The albedo contrast of the wind streaks relative to their surroundings is interpreted to be formed by fine size (bright) and coarser (dark) particles. The formation of the bright wind streaks might be due to the preferential removal of the fine and small particles. The wind streaks also encompass yardangs, which appear extremely long and thin (Figures 19d and 19e), measuring up to ~10 km long and no more than 20 m wide.

Albedo structures associated with aeolian origin were first observed on Mars in the 1970s [*Sagan et al.*, 1972]. *Thomas et al.* [1984] identified, using Viking images, more than 9000 wind streaks on Mars, which are distributed asymmetrically almost entirely in low and middle latitudes [*Thomas and Veverka*, 1979; *Veverka et al.*, 1981; *Thomas et al.*, 1984; *Greeley et al.*, 1993], although they were detected as well outside equatorial regions, at 71°N and 62°S [*Thomas et al.*, 1981]. Wind streaks are common on Mars and comprise a variety of sizes, shapes, and topographic locations, but all of them are largely stable features formed by localized strong winds [*Thomas et al.*, 1981]. Bright streaks on Mars are generally found in bowl-shaped craters [*Arvidson*, 1974] and have elongated forms [*Sagan et al.*, 1972]. These wind morphologies on Mars were reported to be extremely stable, as they are located in areas subject to strong topographic winds [*Thomas and Veverka*, 1979]. The material deposited in the bright streaks on Mars probably consists of fine particles of only a few μm in size [*Pollack et al.*, 1979]. An example of wind streaks on Mars can be seen in Figure 19f, where the bright streaks of ~60 km long indicate the relative constant, unidirectional, and near-surface strong winds.

As opposed to the ongoing studies in planetary aeolian morphologies [*Zimbelman*, 1986; *Bourke et al.*, 2010, Craddock, 2012; *Zimbelman et al.*, 2013], wind streaks on Earth are relatively unexplored and understudied [*Cohen-Zada et al.*, 2016]. Because of the presence of liquid water and vegetation on Earth, many aspects of aeolian erosion are much harder to assess when compared to Mars [*Cohen-Zada et al.*, 2016]. In addition, differences in atmospheric properties between Earth and Mars lead to differences in the observed wind streaks, and thus their interpretation. But still, the aeolian morphologies on Earth are potential paleoclimate proxy indicators [*Li et al.*, 2016] and a comprehensive research of wind streaks on Earth is crucial for our understanding of wind streaks on other planets [*Cohen-Zada et al.*, 2016]. Very few studies about wind streaks on Earth have been conducted. Radar-visible wind streaks were identified by *Landheim et al.* [1992] in Saudi Arabia, Afghanistan, Libya, Chad, China, Russia, and Syria. Wind streaks in the Western Desert of Egypt were compared to those in Cerberus and Elysium Mons on Mars [*El-Baz et al.*, 1979; *El-Baz and Maxwell*, 1979]. In the 1980s, wind streaks were identified I the Altiplano, Bolivia [*Greeley et al.*, 1989]. In 1990s, two wind streaks in the Mojave Desert were reported [*Zimbelman and Williams*, 1996] with the purpose of understanding their formation and evolution. In more recent work, wind streaks from volcanic craters in Patagonia, Argentina, were described [*Rodríguez et al.*, 2010] to improve the understanding on wind streaks in Arabia Terra on Mars. However, the poorly studied wind streaks on Earth raise doubts about their formation; consequently, there is no, to date, geomorphological definition of them, and those already stated in the literature rely almost entirely in orbital observations [*Cohen-Zada et al.*, 2016].

The extremely long and thin yardangs in the Qaidam Basin, together with wind streaks formed by extremely strong unidirectional winds, are unique. No report has been published to date on the strength of winds to form such long structures in the Qaidam Basin. The wind streaks present an unexploited chance to expand our knowledge of their formation and evolution. Wind streaks are important features to provide information of the interaction between the surface and the atmosphere, on past climates, and on evolution of climates. The Qaidam Basin is a natural laboratory for testing the physics of wind processes in an environment rare to Earth and very unique and common to Mars. Our future work will include field investigations of such features and a comparison to their Martian counterparts.

4.1.9. Gravel Deposition

Gravels ranging from millimeters to centimeters in sizes were observed in valleys and on top of small hills in the mountain area of the Qaidam Basin (Figure 20a). These gravels, with chert as the most common mineral, are positioned on top of clay soils, have a rounded nature, suggesting that the area was once a fluvial sedimentary environment, although wind probably plays a role too in the preferential removal of fine particles. The presence of the gravels on higher areas is evidence of granular convection processes as a result of freeze-thaw processes (Figure 20b). When the frozen water in the upper mountain crests thaws, smaller gravel and silicate particles settle in the voids below (Figure 20c) while the larger gravels remain on top. The variably rounded nature of the gravels is an indicator that the abrasion happened over longer periods of time and by fluvial processes. The recent discovery of rounded pebbles by the Curiosity rover in Gale crater presents some of the most significant evidence of sustained fluvial activity on Mars [*Williams et al.*, 2013; *Szabo et al.*, 2015]. Deposits of rounded pebbles were detected in several sites ranging from millimeters to centimeters in diameter [*Yingst et al.*, 2013; *Williams et al.*, 2013]. Based on terrestrial studies, *Williams et al.* [2013] suggest that those Martian rounded pebbles traveled several kilometers to produce the observed rounding, confirming that the climatic conditions on Mars had to be wetter than today.

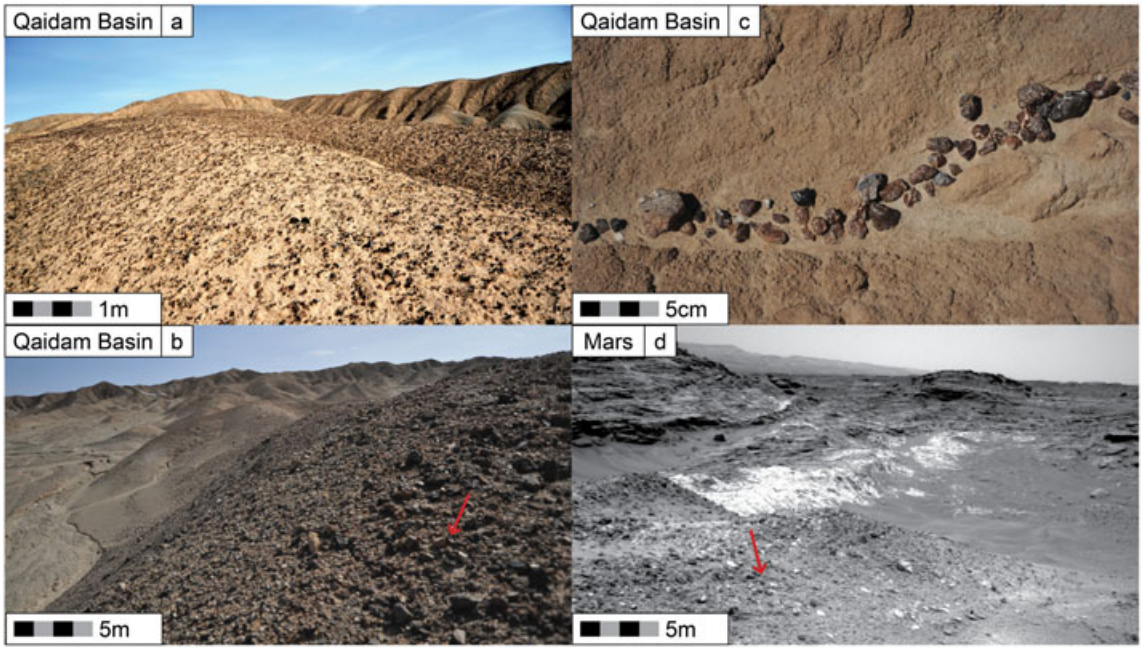

Figure 20. Gravel deposition. (a and b) Extensive gravel plains in the Qaidam Basin. The red arrow indicates the granular convection processes that the area experienced, where larger gravels remain on higher areas. The pictures were taken approximately at 38.33°N, 90.79°E. (c) The small gravels are stored in the small cracks when the water from the upper parts of the mountains thaws. (d) NASA's Curiosity Mars rover on top of a hill 22 meter high near 5.4°S, 137.8°E [NASA/JPL-Caltech]. The scale bars for the pictures are for the nearest place in the bottom of the picture.

On Mars, granular convection processes are also observed where sediments have undergone similar processes [*Szabo et al.*, 2015] (Figure 20d). One considerable difference is that Martian gravels are basaltic in composition [*Szabo et al.*, 2015] rather than the quartz gravels that characterize the Qaidam Basin; however, both cases manifest strong evidence of past fluvial activity where granular convection processes have occurred. Important differences have to be taken into consideration, such as the reduced gravity on Mars in the formation of rounded pebbles [*Komar*, 1980], or flow conditions, horizontal velocity and settling velocity initial particle shapes or the type of fluid [*Szabo et al.*, 2015]; however, despite these differences we can suggest that the pebbles in the Qaidam Basin are another indicator of an ancient wetter environments. The pebbles are also an indicator of aeolian settings, as their shapes give clues on the dust production that results from sand abrasion [*Jerolmack and Brzinski*, 2012; *Bullard et al.*, 2004]. Determining how far these pebbles have traveled and how much abrasion they had experienced could significantly improve our knowledge of paleoenvironments that were wetter and warmer than the current hyperarid conditions.

4.1.10. Dune Fields

In the southeastern part of the western Qaidam Basin where the winds are strong enough to modify the original landscape, the intense effectiveness of aeolian erosion forms abundant dunes and drifts. The morphology of the dunes in the Qaidam Basin is entirely controlled by the availability of sand and wind patterns due to the lack of a vegetation cover. Previous studies already included investigations of the formation, evolution, sedimentology, and geometric shapes of dunes in the Qaidam Basin [*Hesp et al.*, 1989; *Zhou et al.*, 2012; *Yu et al.*, 2015]. In the western Qaidam Basin, barchan dunes (Figure 21a) are the most widespread. Wind-facing slopes are eroded by unidirectional winds and are indicated by the single slip face. Their widths range from 50 to 400 m and are found in areas rich in sand sources. The barchan dune fields are several kilometers long, overlaying in some areas well-bedded saline sediments. Barchan dunes in the Qaidam Basin are majorly composed of sand together with clayish materials, gypsum and halite. While on Mars, in the vicinity of the Viking landing site, the deposits were interpreted to be iron-rich clay, in between other possibilities [*Arvidson et al.*, 1989]. Now they are known to be basaltic minerals; however, sulfate-rich particles may also be present, as they have been detected at Meridiani and interpreted to be dunes of sulfate-cemented muds from ancient playas [*Grotzinger et al.*, 2005; *McLennan et al.*, 2005].

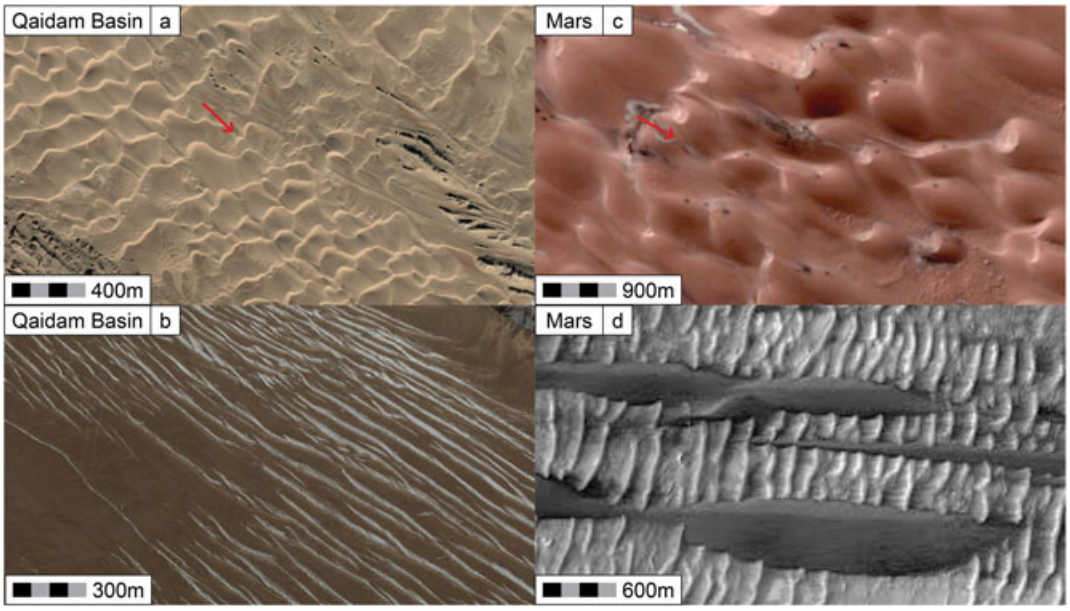

Figure 21. Dune fields. (a) The rhythmic layering is due to effects on the wind on former layered features, forming subsequent sediment mounds, or ripples at 38.37°N, 91.63°E in the Qaidam Basin. The dunes display a single slip face from the top left. The red arrow indicates the direction of the wind. The altitude is 2878 m. (b) Dunes at a location 38.15°N, 91.19°E in the Qaidam Basin. The altitude is 2879 m. (c) Dunes displaying wind directions on a location near 83°50′S, 118° 70′W on Mars [NASA/JPL/University of Arizona]. (d) HiRISE image of dunes in Valles Marineris near 13.9°S, 59.2°W [NASA/JPL/University of Arizona].

Linear dunes (Figure 21b) are less common in the western Qaidam Basin, and they tend to occur in close proximity to barchan dunes. Linear dunes in the western Qaidam Basin are northwest trending and range from a few hundred meters to several kilometers long. Their widths vary from 20–200 m and 10–50 m of separation in between them. Linear dunes are considered to be of depositional origin and formed by stabilized sand under unidirectional winds or by loose sand under bidirectional winds [*Tsoar*, 1989; *Lancaster*, 2009; *Rubin and Hesp*, 2009], although the relationship between their shapes and wind regimes on Earth is still under debate [*Cooke et al.*, 1993; *Lancaster*, 2009; *Parteli et al.*, 2009; *Tokano*, 2010].The linear dunes are thought to be composed of high contents of total silt, clay, and salt, which can stabilize loose sands to form shelters and produce subsequent deposition [*Rubin and Hesp*, 2009]. However, *Zhou et al.* [2012] proposed that the linear dunes in the Qaidam Basin were of erosional origin, instead of depositional origin, based on their analysis of dune internal structures, sediments, and optically stimulated luminescence dating. *Hesp et al.* [1989] reported that linear dunes in the Qaidam Basin undergo southward lateral migration at rates of 3 m/yr, which is the largest reported value to date for linear dune migration on Earth and thus has been cited widely to exemplify the lateral migration of linear dunes [*Rubin*, 1990, *Tsoar et al.*, 2004; *Munyikwa*, 2005; *Livingstone et al.*, 2007].

The Martian equivalents of barchan dunes and linear dunes are displayed in Figures 21c and 21d, respectively. Dunes and megaripples are very common on Mars [*Greeley et al.*, 1981; *Malin et al.*, 1998*; Hayward et al.*, 2007; *Carr*, 2006; *Bourke et al.*, 2010; *Cardinale et al.*, 2012]. They are suggested to be active landforms in the present day [*Bridges et al.*, 2012; *Cardinale et al.*, 2016]. Prior to Mars Reconnaissance Orbiter (MRO) data, Martian imagery showed no evidence of dune motion, which was consistent with climate models indicating that winds capable of moving sand were infrequent in the ~6 mbar atmosphere [*Arvidson et al.*, 1983; *Almeida et al.*, 2008]. However, with increasing imagery resolution of MRO and HiRISE, *Bridges et al.* [2012] were able to show that many dunes and sand ripples on Mars move as much as a few meters per year, proving that the sand on Mars is migrating under current climatic conditions. Their results show that winds in the current low-density Martian atmosphere are strong enough to move ripples and dunes in many locations of the planet. In this contribution, the dunes in the Qaidam Basin could serve as proxies to study the interaction between the wind and the atmosphere. Their movements, orientations, shapes, sand properties, and wind force may be used to infer aspects of the active dunes on Mars.

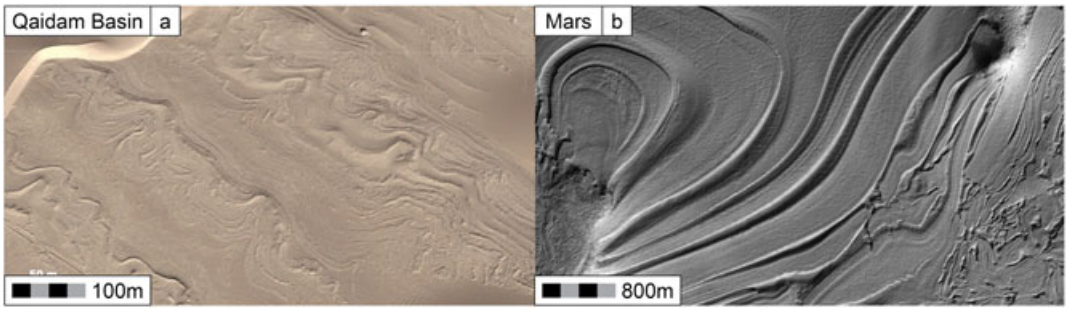

Figure 22. Swirling structures. (a) The swirling textures suggest that the distributary channels are possibly the result of interaction between water and waterlogged sediments. The layers appear folded or deformed as they possibly had to adjust to the additional weight of subsequent deposition. Image at 37.72°N, 92.88°E. The altitude is 3070 m. (b) HiRISE image of wavy layers in Hellas Planitia at 40°S, 52°E [NASA/JPL/University of Arizona].

4.1.11. Swirling Textures

Small swirling patterns appear in some locations in the Qaidam Basin. The interpretation of these features indicates something of the nature of surficial conditions and processes. We speculate that the honeycomb patterns are impressions made by mountain runoff water-ice blocks grounding into initially soft mud, composed mainly of silt, clay, and salts. The area where these honeycomb patterns appear is in the piedmont of the mountain area in the southwestern part of the Qaidam Basin, where dune fields are present. The location is therefore a collector of runoff water-ice, tectonic movements, and eolian sediment, although an issue is the relative importance of each eolian, tectonic, and aqueous processes. The patterns suggest that at least pressure, occasional precipitation, surface runoff, and temperature conditions at the surface were in equilibrium and allowed water to be stabilized. Figure 22a displays furrowed or swirling textures in the western Qaidam Basin.

Noachian terrains on Mars display similar features, although much larger and deeper in size, where large floods were rare [*Cabrol and Grin*, 2010]. For instance, on the floor of the impact crater Hellas, the sediments were suggested to be deposited in ice-covered water, degraded later when ice decayed and finally eroded by wind [*Moore and Wilhelms*, 2001]. The swirling textures on Hellas suggest a deformation created by the interaction of ephemeral runoff together with waterlogged sediments and ice [*Cabrol and Grin*, 2010] (Figure 22b). Additional supportive evidence of materials consistent with lacustrine origin in Hellas comes from the thermal and midinfrared spectroscopic mapping [*Moore and Wilhelms*, 2001]. Thermal inertia of Hellas Planitia indicated that the coarsest material was not larger than dust or sand [*Moore and Edgett*, 1993].

We speculate that the patterns created in the Qaidam Basin have some similarity to those found on Hellas, despite the differences in size and the numerous differences in climatic conditions. We believe that the observed topographic patterns imply at least one relatively well-defined water body and surficial runoff. We certainly accept that our speculation of the patterns, as an explanation, is not conclusive. Both scenarios on Hellas and the Qaidam Basin are consistent with the plausible failure to transport large amounts of saturated sediments. The extensive occurrence of phyllosilicates in Noachian landscapes, together with the evidence of surface water transport, suggests at least occasional warmer conditions during the Noachian [*Grotzinger et al.*, 2005]. Although it seems that liquid water was stabilized at the end of the Noachian (as it can be proved by the geomorphic and mineralogical evidence), such conditions still remain unclear [*Cabrol and Grin*, 2010]. This discrepancy is one of the most mysterious aspects of Mars' evolution. This is a brief and preliminary comment about these patterns, which will undoubtedly be a subject of more detailed study.

4.2. Tectonic Features

4.2.1. Ring Structures

Ring structures are identified in the saline lake facies of Xiaoliang, Nanyi, Jianding, and Honggouzi Mountains (see Figure 2). The ring structures are tectonic anticlines that form a mound with a fine symmetrical stratification which is interpreted to contain alternating layered deposits of darker clay-rich (mainly gypsum) and brighter salt-rich (mainly halite) material embedded in clay, which were deposited from the drying of the

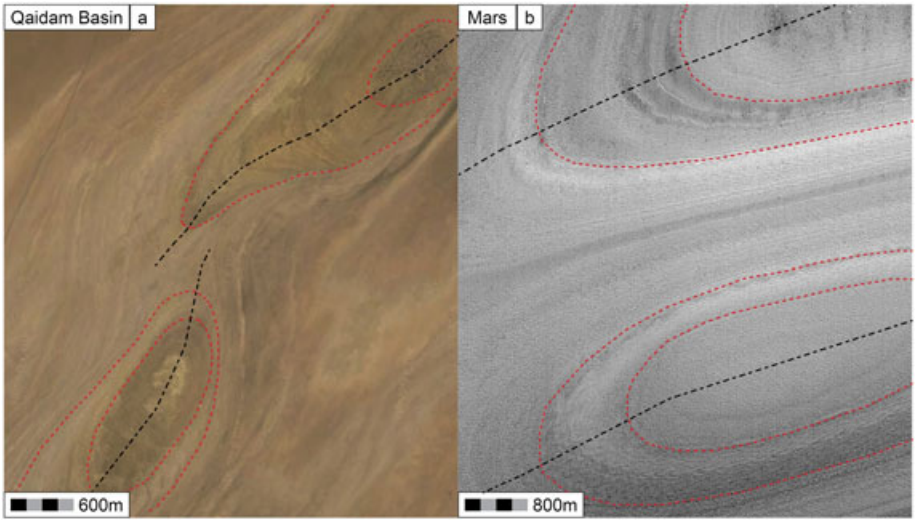

Figure 23. Ring structures. (a) Pairs of ring structures in the Qaidam Basin at 38.49°N, 91.74°E with an altitude of 2742 m. (b) MOC image MOC2–1512 of a pair of Ring Structures on the Martian northern polar region at 85.70°N, 21.00°W [*Anglés and Li*, 2016]. Original image from NASA/JPL-Caltech/Malin Space Science Systems.

brines [*Anglés and Li*, 2016]. The enclosed nature of these structures is due to the surrounding thrust belts that cause the salts to rise and create new layers [*Anglés and Li*, 2016]. These structures offer a unique analogy to Martian ring structures observed in the northern polar region. Martian ring structures exhibit small layered hills that resulted from the surface manifestation of surrounding folds that accommodate the salt rocks similar to those in the Qaidam Basin [*Anglés and Li*, 2016].

Pairs of ring structures in the Qaidam Basin (Figure 23a) bear a strong resemblance to pairs of ring structures observed in the Martian northern polar region (Figure 23b). They are the result of fault compression forces that created the structure and eventually fractured it into two in a direction perpendicular to the compression [*Anglés and Li*, 2016]. Both the Martian northern polar region and the Qaidam Basin show thrusts that cut the layers in the edge of the ring structures, indicating a recent tectonic pressurization of the salts.

5. Habitability

In practically all deserts of Earth, photosynthetic microorganisms occupy hypolithic or endolithic habitats [*Wynn-Williams*, 2000]. Hypolithic cyanobacteria grow underneath translucent rocks, whereas endolithic cyanobacteria grow inside the pore spaces of rocks [*Wierzchos et al.*, 2006].

Many terrestrial analogues are characterized by challenging conditions for terrestrial life, such as low temperatures, extremes of salinity, and pH [*Fairén et al.*, 2010]. Through the study of terrestrial analogues, we gain crucial information with respect to the ability of organisms to survive extreme conditions, as well as to the limits of life on Earth [*Fairén et al.*, 2010]. Previous studies already analyzed microbial populations on Mars analogue environments [e.g., *Fernández-Remolar et al.*, 2005; *Clarke*, 2006; *Edwards et al.*, 2007; *Fernández-Remolar et al.*, 2008; *Foing et al.*, 2011; *Fernández-Remolar et al.*, 2013]. The Atacama desert, considered one of the most similar places on Earth to Mars [*Navarro-González et al.*, 2003], contains endolithic microorganisms within halite rocks [*Wierzchos et al.*, 2006]. *Wierzchos et al.* [2006], analyzed endolithic photosynthetic life within halite rocks as an analogue for the evaporite rocks on Mars.

However, the many Mars analogue sites previously studied only represent some aspects of the present Mars conditions, and thus, further analysis in new Mars analogues is still meaningful.

The Qaidam Basin is one of the driest deserts on Earth and provides an assessment of life forms that have the ability to survive the extreme climatic conditions that characterize the basin. There are no visible life forms on rock surfaces or on soil; however, previous microbial studies detected halophiles as the most abundant archaea in the Qaidam Basin by analyzing sediment cores [*Wang et al.*, 2013]. We also identified hypolithic microbial communities living under translucent stones (Figures 24b and 24c). The specimens were located at ~3028 m in elevation on the southwest of the Qaidam Basin at approximately 38.29°N, 90.85°E, along

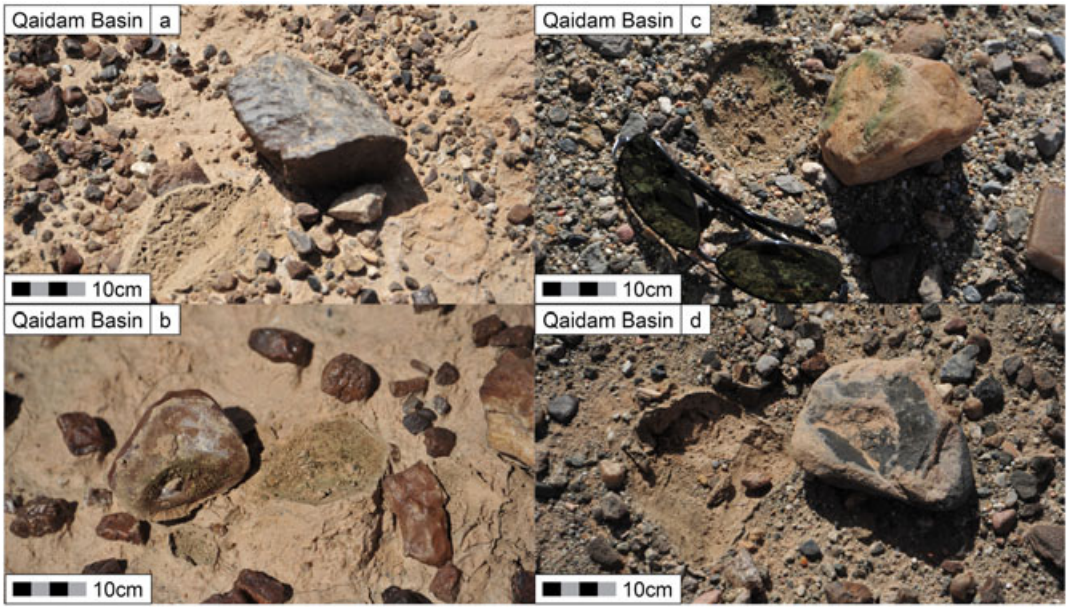

Figure 24. Hypolithic photosynthesis. (a) Hypolithic niches of photosynthesis were not found below rocks in the clay compacted mountain area. Note the lack of cyanobacteria (green color) beneath the rock. (b) Microbial mats were only found under transparent chert rocks in the Qaidam Basin. (c) Microbial mat on the lower part of a chert rock. (d) Absence of microbial mat on an opaque rock in the Qaidam Basin.

~150 m within the confines of the mountain area and an extended fluvial fan (Figure 25, "b" area). Their distribution appears most strongly to be regulated by small amounts of retained water from underneath that can be sustained thanks to the chert rocks. Nearly all transparent chert rocks in the area harbor microbial colonization, although it was confined to rocks pieces of ~10–15 cm wide. These rocks are sufficiently translucent to filter the strong UV radiation but allow photosynthetic visible lights to penetrate and allow them to retain enough moisture to support photosynthesis [*Cockell and Stokes*, 2006]. The thermal inertia of the rock allows the environment underneath to be protected from the outer dry and cold temperature that characterizes the Qaidam Basin, moderating the temperature of the hypolithic community at all seasons [*Schlesinger et al.*, 2003]. Once sheltered from the environmental extremes of the basin, these hyperarid adapted microorganisms are sufficient in terms of the level of radiation and organic

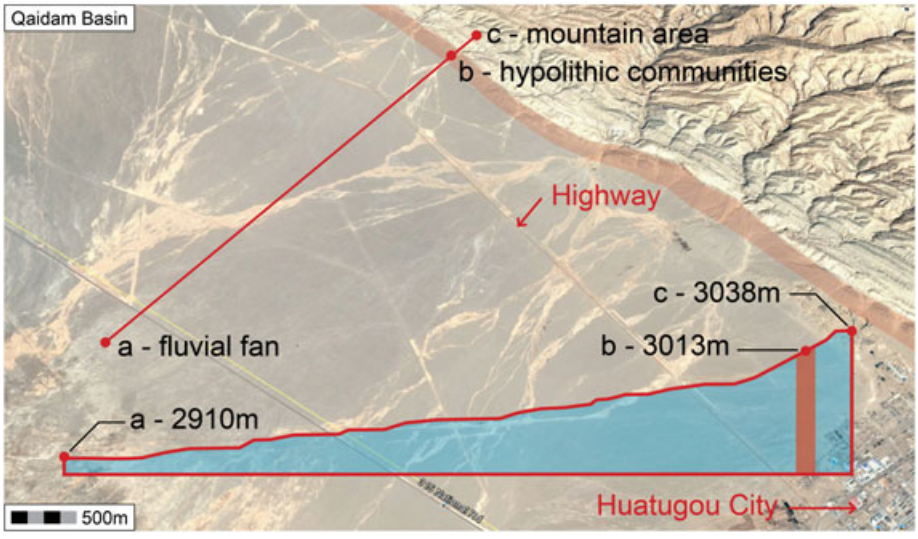

Figure 25. Hypolithic photosynthesis. The image displays the narrow area where the photosynthetic communities were found. Approximate location of b is at 38.29°N, 90.85°E at an altitude of 3013 m.

material required to survive in such habitat. On the contrary, photosynthesis did not take place beneath opaque rocks (Figures 24a and 24d) as no radiation could penetrate the rock to sustain microbial niche beneath it.

Hypolithic niches of photosynthesis were only found in the area between the fluvial fan and mountain area (Figure 25) in the most southwestern part of the Qaidam Basin. The fluvial fan (Figure 25, "a" area) is characterized by millimeter sized particles of quartz (less than 0.5 cm), hardly possible to retain any water or sustain any microbial life. The upper mountain area (Figure 25, "c" area) is characterized by majorly clays and salts with little pore structure that prevent the transportation of water to the near surface due to the strong evaporation after precipitation. The mountain area does not sustain any hypolithic niche because of the high compaction of clay deposition that does not allow the transportation of water to the surface (Figure 24a). The combined result of Figures 24 and 25 indicates that water is not collected from the atmosphere but from underground.

Laboratory investigations of the hypolithic communities found embedded in ground are currently being carried out, and they will be reported in a future publication. The results will have meaningful biological insight into the possibility of hypolithic photosynthetic microbial communities on Mars, despite the environmental differences, physical and chemical regimes between the Martian surface and those observed in the Qaidam Basin.

6. Conclusions

The unique resemblance of current hyperarid conditions, high UV radiation, low atmospheric pressure, saline environments, and overall geomorphological features in the Qaidam Basin and on Mars is exceptional. In both Mars and the Qaidam Basin, considerable amounts of groundwater and consistent aeolian processes acted on the upper layers of the lithology carving elaborate patterns into the surface. Today, landscapes are dominated by strong weathering and hyperarid conditions, where minerals and weathering processes coexist in adjacent proximity. Much may be gained from this interaction, such as a better understanding of the Martian surface from analyzing the sedimentary and weathering environments in the hyperarid systems of north Tibetan Plateau.

Mineralogical compositional analyses from SEM and XRD of the Qaidam Basin confirm that the depositional materials are rich in sulfate, followed by halite and clay minerals. There are a variety of clays together with chlorides, attesting to an important role of past water. The results suggest saturated sulfate solutions and precipitation resulting from evaporation of brines, which is of great interest for Mars mineralogy as magnesium sulfates, calcium sulfates, and polyhydrate sulfates have been detected at many Martian locations. Large deposits of gypsum and halite that form the saline lake deposits in the Qaidam Basin are comparable to those sulfate deposits detected on the Martian surface. The TG analysis gives us important information on the amount of water molecules in pure gypsum samples; 20% of water is contained in the crystals, and this has a direct implication to the gypsum deposits on Mars. Our future work will provide a better understanding of how the heating of gypsum could be of great importance to obtain water for future missions to Mars. The adaptive mechanisms of hypolithic organisms to survive the environmental extremes in the Qaidam Basin can also contribute to an understanding of extremophiles, and it is directly relevant to any possible life on Mars. The immense size of the Qaidam Basin is also of extreme importance for future Mars exploration programs. Rovers can explore their capabilities and drive in real time with extreme hyperarid conditions. The practice of sample acquisition, detection of obstacles, and movement though abrupt surfaces will provide valuable information for the exploration of future targets on Mars. The Qaidam Basin is a realistic environment that replicates the distribution of features and materials that the vehicles will find on the Martian surface.

We suggest that many geomorphological structures on Mars may have been formed by similar processes, as they are analogous to those displayed in the Qaidam Basin. While the processes and resulting geomorphological landforms on the Qaidam Basin provide a feasible analogue to the Martian topography and its structures, it is recognized that the exact Martian conditions are not characterized. Nevertheless, given the similarities that the Qaidam Basin contains, especially around the climate, aridity, and hydrology, this area may be a valuable potential terrestrial analogue to study modern Martian processes, landforms, and microorganism preservation potential and can be treated as an important site for confirming future Mars sample return missions.

Acknowledgments

This study was supported by the General Research Fund (HKU702913P) from the Research Grants Council of Hong Kong and the Earth as a Habitable Planet Thesis Development Grant, from The University of Hong Kong. The imagery data used for Mars are available at NASA and ESA. We thank Feng Qing Han of Qinghai Institute of Salt Lakes of the Chinese Academy of Sciences for his support for field trips to the Qaidam Basin and James Stewart for his assistance in the technical editing of the manuscript.

References

Almeida, M. P., E. J. R. Parteli, J. S. Andrade, and H. J. Hermann (2008), Giant saltation on Mars, *Natl. Acad. Sci. Proc.*, *105*, 6222–6226, doi:10.1073/pnas.0800202105.

Anderson, R. B., and J. F. Bell (2010), Geologic mapping and characterization of Gale Crater and implications for its potential as a Mars science laboratory landing site, *Marsyas*, *5*, 76–128, doi:10.1555/mars.2010.0004.

Anglés, A., and Y. L. Li (2016), Similar ring structures on Mars and Tibetan Plateau confirm recent tectonism on Martian northern polar region, *Astrobiology*, 1–5, doi:10.1017/S1473550416000446.

Arvidson, R. E. (1974), Wind-blown streaks, splotches, and associated craters on Mars: Statistical analysis of Mariner 9 photographs, *Icarus*, *21*(1), 12–27, doi:10.1016/0019-1035(74)90086-4.

Arvidson, R. E., J. L. Gooding, and H. J. Moore (1989), The Martian surface as imaged, sampled, and analyzed by the Viking landers, *Rev. Geophys.*, *27*, 39–60, doi:10.1029/RG027i001p00039.

Arvidson, R. E., E. A. Guinness, H. J. Moore, J. Tillman, and S. D. Wall (1983), Three Mars years: Viking Lander 1 imaging observations, *Science*, *222*, 463–468, doi:10.1126/science.222.4623.463.

Arvidson, R. E., F. Poulet, J. P. Bibring, M. Wolff, A. Gendrin, R. V. Morris, J. J. Freeman, Y. Langevin, N. Mangold, and G. Bellucci (2005), Spectral reflectance and morphologic correlations in eastern Terra Meridiani, Mars, *Science*, *307*(5715), 1591–1594, doi:10.1126/science.1109509.

Baker, V. R., and D. Nummedal (1978), The channeled scabland: A guide to the geomorphology of the Columbia Basin, Washington: (Prepared for the Comparative Planetary Geology Field Conference held in the Columbia Basin, June 5–8, 1978), edited by V. R. Baker and D. Nummedal, 186 pp., US National Aeronautics and Space Administration, Washington, D. C.

Baldridge, A. M., J. D. Farmer, and J. E. Moersch (2004), Mars remote-sensing analog studies in the Badwater Basin, Death Valley, California, *J. Geophys. Res.*, *109*, E12006, doi:10.1029/2004JE002315.

Balme, M., N. Mangold, D. Baratoux, F. Costard, M. Gosselin, P. Masson, P. Pinet, and G. Neukum (2006), Orientation and distribution of recent gullies in the southern hemisphere of Mars: Observations from High Resolution stereo Camera/Mars Express (HRSC/MEX) and Mars Orbiter Camera/Mars Global Surveyor (MOC/MGS) data, *J. Geophys. Res.*, *111*, E05001, doi:10.1029/2005JE002607.

Benison, K. C. (2006), A Martian analogue in Kansas: Comparing Martian strata with Permian acid saline lake deposits, *Geology*, *34*(5), 385–388, doi:10.1130/G22176.1.

Benison, K. C., and D. A. LaClair (2003), Modern and ancient extremely acid saline deposits: Terrestrial analogs for Martian environments?, *Astrobiology*, *3*(3), 609–618, doi:10.1089/153110703322610690.

Bishop, J. L., E. Z. N. Dobrea, N. K. McKeown, M. Parente, B. L. Ehlmann, J. R. Michalski, R. E. Milliken, F. Poulet, G. A. Swayze, and J. F. Mustard (2008), Phyllosilicate diversity and past aqueous activity revealed at Mawrth Vallis, Mars, *Science*, *321*(5890), 830–833, doi:10.1126/science.1159699.

Blondel, P., and J. W. Mason (2006), *Solar System Update*, pp. 135–158, Springer, Berlin.

Bourke, M. C., N. Lancaster, L. K. Fenton, E. J. R. Parteli, J. R. Zimbelman, and J. Radebaugh (2010), Extraterrestrial dunes: An introduction to the special issue on planetary dune systems, *Geomorphology*, *121*, 1–14, doi:10.1016/j.geomorph.2010.04.007.

Bourke, M. C., and J. Zimbelman (2001), The Australian paliofloood model for unconfined fluvial deposition on Mars, *32nd Lunar and Planetary Science Conference*, 1679.

Bridges, N. T., et al. (2012), Planet-wide sand motion on Mars, *Geology*, *40*(1), 31–34, doi:10.1130/G32373.1.

Brown, A. J., M. R. Walter, and T. J. Cudahy (2005), Hyperspectral imaging spectroscopy of a Mars analogue environment at the North Pole Dome, Pilbara Craton, Western Australia, *Aust. J. Earth Sci.*, *52*(3), 353–364, doi:10.1080/08120090500134530.

Bullard, J. E., G. H. McTainsh, and C. Pudmenzky (2004), Aeolian abrasion and modes of fine particle production from natural red dune sands: An experimental study, *Sedimentology*, *51*(5), 1103–1125, doi:10.1111/j.1365-3091.2004.00662.x.

Cabrol, N. A., and E. A. Grin (2001), The evolution of lacustrine environments on Mars: Is Mars only hydrologically dormant?, *Icarus*, *149*(2), 291–328, doi:10.1006/icar.2000.6530.

Cabrol, N. A., and E. A. Grin (2010), *Lakes on Mars*, pp. 31–270, Elsevier, Netherlands.

Cardinale, M., G. Komatsu, S. Silvestro, and D. Tirsch (2012), The influence of local topography for wind direction on Mars: Two examples of dune fields in crater basins, *Earth Surf. Process. Landf.*, *37*(13), 1437–1443, doi:10.1002/esp.3289.

Cardinale, M., S. Silvestro, D. A. Vaz, T. Michaels, M. C. Bourke, G. Komatsu, and L. Marinangeli (2016), Present-day aeolian activity in Herschel crater, Mars, *Icarus*, *265*, 139–148, doi:10.1016/j.icarus.2015.10.022.

Carr, M. H. (1996), *Water on Mars*, pp. 30–210, Oxford University Press, New York.

Carr, M. H. (2006), *The Surface of Mars*, pp. 113–265, University Press, Cambridge, U. K.

Chan, M. A., P. W. Jewell, T. J. Parker, J. Ormo, C. H. Okubo, and G. Komatsu (2016), Pleistocene Lake Bonneville as an analog for extraterrestrial lakes and oceans, in *Lake Bonneville: A Scientific Update Developments in Earth Surface Processes*, 20, edited by C. G. Oviatt and J. F. Shroder, pp. 570–597, Elsevier, Amsterdam, doi:10.1016/B978-0-444-63590-7.00021-4.

Chevrier, V. F., and E. G. Rivera-Valentin (2012), Formation of recurring slope lineae by liquid brines on present-day Mars, *Geophys. Res. Lett.*, *39*, L21202, doi:10.1029/2012GL054119.

Christensen, P. R. (2003), Formation of recent Martian gullies through melting of extensive water-rich snow deposits, *Nature*, *422*(6927), 45–48, doi:10.1038/nature01436.

Clarke, J. D. (2006), A multi-goal Mars analogue expedition (expedition two) to the Arkaroola region, Australia, *Mars Anal. Res. Sci. Tech. Ser.*, *111*, 3–15.

Cockell, C. S., and M. D. Stokes (2006), Hypolithic colonization of opaque rocks in the Arctic and Antarctic polar desert, *Arct. Antarct. Alp. Res.*, *38*(3), 335–342, doi:10.1657/1523-0430(2006)38.

Cohen-Zada, A. L., D. G. Blumberg, and S. Maman (2016), Earth and planetary Aeolian streaks: A review, *Aeolian Res.*, *20*, 108–125, doi:10.1016/j.aeolia.2015.12.002.

Connerney, J., M. Acuna, P. J. Wasilewski, N. F. Ness, H. Reme, C. Mazelle, D. Vignes, R. Lin, D. Mitchell, and P. Cloutier (1999), Magnetic lineations in the ancient crust of Mars, *Science*, *284*(5415), 794–798, doi:10.1126/science.284.5415.794.

Cooke, R., A. Warren, and A. Goudie (1993), *Desert Geomorphology*, pp. 23–44, UCL Press, London.

Costard, F., F. Forget, N. Mangold, and J. P. Peulvast (2002), Formation of recent Martian debris flows by melting of near-surface ground ice at high obliquity, *Science*, *295*(5552), 110–113, doi:10.1126/science.1066698.

Craddock, R. A. (2012), Aeolian processes on the terrestrial planets: Recent observations and future focus, *Prog. Phys. Geogr.*, *36*(1), 110–124, doi:10.1177/0309133311425399.

De Hon, R. (1992), Martian lake basins and lacustrine plains, *Earth Moon Planet.*, *56*(2), 95–122, doi:10.1007/BF00056352.

De Silva, S., J. Bailey, K. Mandt, and J. Viramonte (2010), Yardangs in terrestrial ignimbrites: Synergistic remote and field observations on Earth with applications to Mars, *Planet. Space Sci.*, *58*(4), 459–471, doi:10.1016/j.pss.2009.10.002.

Di Achille, G., and B. M. Hynek (2010), Ancient ocean on Mars supported by global distribution of deltas and valleys, *Nat. Geosci.*, *3*(7), 459–463, doi:10.1038/ngeo891.

Dickson, J. L., J. W. Head, J. S. Levy, and D. R. Marchant (2013), Don Juan Pond, Antarctica: Near-surface $CaCl_2$-brine feeding Earth's most saline lake and implications for Mars, *Sci. Rep.*, *3*(1166), 1–7, doi:10.1038/srep01166.

Dickson, J. L., J. W. Head, and D. R. Marchant (2008), Late Amazonian glaciation at the dichotomy boundary on Mars: Evidence for glacial thickness maxima and multiple glacial phases, *Geology*, *36*(5), 411–414, doi:10.1130/G24382A.1.

Diniega, S., S. Byrne, N. T. Bridges, C. M. Dundas, and A. S. McEwen (2010), Seasonality of present-day Martian dune-gully activity, *Geology*, *38*, 1047–1050, doi:10.1130/G31287.1.

Dohm, J. M., et al. (2011), An inventory of potentially habitable environments on Mars: Geological and biological perspectives, *Geol. Soc. Am. Spec. Pap.*, *483*, 317–347, doi:10.1130/2011.2483(21).

Dundas, C. M., S. Diniega, C. J. Hansen, S. Byrne, and A. S. McEwen (2012), Seasonal activity and morphological changes in Martian gullies, *Icarus*, *220*, 124–143, doi:10.1016/j.icarus.2012.04.005.

Dundas, C. M., A. S. McEwen, S. Diniega, S. Byrne, and S. Martinez-Alonso (2010), New and recent gully activity on Mars as seen by HiRISE, *Geophys. Res. Lett.*, *37*, L07202, doi:10.1029/2009GL041351.

Edwards, H. G., P. Vandenabeele, S. E. Jorge-Villar, E. A. Carter, F. Rull Perez, and M. D. Hargreaves (2007), The Rio Tinto Mars analogue site: An extremophilic Raman spectroscopic study, *Spectrochim. Acta A Mol. Biomol. Spectrosc.*, *68*(4), 1133–1137, doi:10.1016/j.saa.2006.12.080.

Ehlmann, B. L., J. F. Mustard, S. L. Murchie, F. Poulet, J. L. Bishop, A. J. Brown, W. M. Calvin, R. N. Clark, D. J. Des Marais, and R. E. Milliken (2008), Orbital identification of carbonate-bearing rocks on Mars, *Science*, *322*(5909), 1828–1832, doi:10.1126/science.1164759.

El Maarry, M., W. J. Markiewicz, M. T. Mellon, W. Goetz, J. M. Dohm, and A. Pack (2010), Crater floor polygons: Desiccation patterns of ancient lakes on Mars?, *J. Geophys. Res.*, *115*, E10006, doi:10.1029/2010JE003609.

El Maarry, M., A. Pommerol, and N. Thomas (2013), Analysis of polygonal cracking patterns in chloride-bearing terrains on Mars: Indicators of ancient playa settings, *J. Geophys. Res. Planets*, *118*, 2263–2278, doi:10.1002/2013JE004463.

El Maarry, M., J. Kodikara, S. Wijessoriya, W. J. Markiewicz, and N. Thomas (2012), Dessication mechanism for formation of giant polygons on Earth and intermediate-sized polygons on Mars: Results from a pre-fracture model, *Earth Planet. Sci. Lett.*, *323*, 19–26, doi:10.1016/j.epsl.2012.01.016.

El-Baz, F., and T. A. Maxwell (1979), Eolian streaks in southwestern Egypt and similar features in the Cerberus region of Mars, *Lunar Planet. Sci. Conf. X*, *3*, 3017–3030.

El-Baz, F., C. Breed, M. Grolier, and J. McCauley (1979), Eolian features in the Western Deser of Egypt and some applications to Mars, *J. Geophys. Res.*, *84*(B14), 8205–8221.

Essefi, E., G. Komatsu, A. G. Fairen, M. A. Chan, and C. Yaich (2014a), Models of formationand activity of springs moundsin the Mechertate-Chrita-Sidi El Hani System, Eastern Tunisia: Implications for the habitabiliy of Mars, *Lifestyles*, *4*(3), 386–432, doi:10.3390/life4030386.

Essefi, E., G. Komatsu, A. G. Fairen, M. A. Chan, and C. Yaich (2014b), Groundwater influence on the aeolian sequence stratigraphy of the Mechertate-Chrita-Sidi El Hani System, Tunisian Sahel: Analogies to the wet-dry aeolian sequence stratigraphy at Meridiani Planum, Terby crater, and Gale Crater, Mars, *Planet. Space Sci.*, *95*, 56–78, doi:10.1016/j.pss.2013.05.010.

Evans, D. J. A., and D. R. Twigg (2002), The active temperature glacial landsystem: A model based on Breioamerkurjokull and Fjallsjokull, Iceland, *Quat. Sci. Rev.*, *21*(20), 2143–2177, doi:10.1016/S0277-3791(02)00019-7.

Fairén, A. G., et al. (2010), Astrobiology through the ages of Mars: The study of terrestrial analogues to understand the habitability of Mars, *Astrobiology*, *10*(8), 821–843, doi:10.1089/ast.2009.0440.

Fairén, A. G., et al. (2014), A cold hydrological system in Gale Crater, Mars, *Planet. Space Sci.*, *93-94*, 101–118, doi:10.1016/j.pss.2014.03.002.

Fang, X., W. Zhang, Q. Meng, J. Gao, X. Wang, J. King, C. Song, S. Dai, and Y. Miao (2007), High-resolution magnetostratigraphy of the Neogene Huaitoutala section in the eastern Qaidam Basin on the NE Tibetan Plateau, Qinghai Province, China and its implication on tectonic uplift of the NE Tibetan Plateau, *Earth Planet. Sci. Lett.*, *258*(1), 293–306, doi:10.1016/j.epsl.2007.03.042.

Fasset, C. I., and J. W. Head (2008), The timing of Martian valley network activity: Constraints from buffered crater counting, *Icarus*, *195*(1), 61–89, doi:10.1016/j.icarus.2007.12.009.

Fernández-Remolar, D. C., R. V. Morris, J. E. Greuner, R. Amils, and A. H. Knoll (2005), The Rio Tinto, Spain: Mineralogy, sedimentary geobiology and implications for interpretation of outcrop rocks at Meridiani Planum, Mars, *Earth Planet. Sci. Lett.*, *240*(1), 149–167, doi:10.1016/j.epsl.2005.09.043.

Fernández-Remolar, D. C., O. Prieto-Ballesteros, N. Rodríguez, F. Gómez, R. Amils, J. Gómez-Elvira, and C. R. Stoker (2008), Underground habitats in the Río Tinto basin: A model for subsurface life habitats on Mars, *Astrobiology*, *8*(5), 1023–1047, doi:10.1089/ast.2006.0104.

Fernández-Remolar, D. C., et al. (2013), Molecular preservation in halite-and perchloraterich hypersaline subsurface deposits in the Salar Grande basin (Atacama Desert, Chile): Implications for the search for molecular biomarkers on Mars, *J. Geophys. Res. Biogeosci.*, *118*, 922–939, doi:10.1002/jgrg.20059.

Foing, B. H., C. Stoker, J. Zavaleta, and P. Ehrenfreund (2011), Field astrobiology research in Moon-Mars analogue environments: Instruments and methods, *Astrobiology*, *10*(3), 141–160, doi:10.1017/S1473550411000036.

Forsythe, R., and C. Blackwelder (1998), Noachian Martian salars (closed drainage salt pans) and sabkhas as lander/sample return mission target, paper presented at *Mars Surveyor 2001 Landing Site Workshop*, Moffett Field, California.

Goudie, A. S. (2007), Mega-yardangs: A global analysis, *Geogr. Compass*, *1*(1), 65–81, doi:10.1111/j.1749-8198.2006.00003.x.

Greeley, R., and J. D. Iversen (1987), *Wind as a Geological Process: on Earth*, *Mars*, *Venus and Titan*, 4, pp. 108–198, Cambridge Univ. Press Archive, Cambridge, U. K.

Greeley, R., B. R. White, J. B. Pollack, J. D. Iversen, and R. N. Leach (1981), Dust storms on Mars: Considerations and simulations, *Geol. Soc. Am. Spec. Pap.*, *186*, 101–122, doi:10.1130/SPE186-p101.

Greeley, R., P. Christensen, and R. Carrasco (1989), Shuttle radar images of wind streaks in the Altiplano, Bolivia, *Geology*, *17*, 665–668, doi:10.1130/0091-7613.

Greeley, R., A. Skypeck, and J. Pollack (1993), Martian aeolian features and deposits-comparison with general circulations model result, *J. Geophys. Res.*, *98*, 3183–3196, doi:10.1029/92JE02580.

Grotzinger, J. P., and R. E. Milliken (2012), The sedimentary rock record of Mars: Distribution, origins, and global stratigraphy, in *Sedimentary Geology of Mars*, *Society for Sedimentary Geology Special Publication*, vol. 102, edited by J. P. Grotzinger and R. E. Milliken, pp. 1–48, SEPM Special Publication, Tulsa, Okla., doi:10.2110/pec.12.102.0001.

Grotzinger, J. P., et al. (2005), Stratigraphy and sedimentology of a dry to wet eolian depositional system, Burns formation, Meridiani Planum, Mars, *Earth Planet. Sci. Lett.*, *240*(1), 11–72, doi:10.1016/j.epsl.2005.09.039.
Gulick, V. C. (2001), Origin of the valley networks on Mars: A hydrological perspective, *Geomorphology*, *37*(3), 241–268, doi:10.1016/S0169-555X(00)00086-6.
Hartmann, W. K., T. Thorsteinsson, and F. Sigurdsson (2003), Martian hillside gullies and Icelandic analogs, *Icarus*, *162*(2), 259–277, doi:10.1016/S0019-1035(02)00065-9.
Hayward, R. K., K. F. Mullins, L. K. Fneton, T. M. Hare, T. N. Titus, M. C. Bourke, A. Colaptrete, and P. R. Christenser (2007), Mars global digital dune database and initial science results, *J. Geophys. Res.*, *112*, E11007, doi:10.1029/2007JE002943.
Head, J. W., and D. R. Marchant (2014), The climate history of early Mars: Insights from the Antarctic McMurdo dry valleys hydrologic system, *Antarct. Sci.*, *26*(06), 774–800, doi:10.1017/S0954102014000686.
Head, J. W., J. F. Mustard, M. A. Kreslavsky, R. E. Milliken, and D. R. Marchant (2003), Recent ice ages on Mars, *Nature*, *426*(6968), 797–802, doi:10.1038/nature02114.
Head, J. W., et al. (2005), Tropical to mid-latitude snow and ice accumulation, flow and glaciation on Mars, *Nature*, *434*(7031), 346–351, doi:10.1038/nature03359.
Hesp, P., R. Hyde, V. Hesp, and Z. Qian (1989), Longitudinal dunes can move sideways, *Earth Surf. Process. Landf.*, *14*, 447–451, doi:10.1002/esp.3290140510.
Hoffman, N., L. P. Knauth, S. Klonowski, D. Burt, R. S. Saunders, R. W. Zurek, P. T. Doran, and S. L. Forman (2000), Ideas about the surface runoff features on Mars, *Science*, *290*(5492), 711–714, doi:10.1126/science.290.5492.711c.
Houston, J. (2006), Evaporation in the Atacama Desert: An empirical study of spatio-temporal variations and their causes, *J. Hydrol.*, *330*(3), 402–412, doi:10.1016/j.jhydrol.2006.03.036.
Howard, A. D., R. C. Kochel, and H. E. Holt (1987), Sapping features of the Colorado Plateau: A comparative planetary geology field guide.
Howard, A. D., J. M. Moore, and R. P. Irwin (2005), An intense terminal epoch of widespread fluvial activity on early Mars: 1. Valley network incision and associated deposits, *J. Geophys. Res.*, *110*, E12S14, doi:10.1029/2005JE002460.
Irwin, R. P., A. D. Howard, R. A. Craddock, and J. M. Moore (2005), An intense terminal epoch of widespread fluvial activity on early Mars: 2. Increased runoff and paleolake development, *J. Geophys. Res.*, *110*, E12S15, doi:10.1029/2005JE002460.
Jakosky, B. M., J. M. Grebowsky, J. G. Luhmann, and D. A. Brain (2015), Initial results from the MAVEN mission to Mars, *Geophys. Res. Lett.*, *42*, 8791–8802, doi:10.1002/2015GL065271.
Jerolmack, D. J., and T. A. Brzinski (2012), Equivalence of abrupt grain-size transitions in alluvial rivers and eolian sand seas: A hypothesis, *Geology*, *38*(8), 719–722, doi:10.1130/G30922.1.
Kapp, P., J. D. Pelletier, A. Rohrmann, R. Heermance, J. Russell, and L. Ding (2011), Wind erosion in the Qaidam basin, central Asia: Implications for tectonics, paleoclimate, and the source of the Loess Plateau, *GSA Today*, *21*(4/5), 4–10, doi:10.1130/GSATG99A.1.
Kargel, J. S. (2004), *Mars-A Warmer, Wetter Planet*, pp. 43–61, Springer, New York.
Kezao, C., and J. M. Bowler (1986), Late Pleistocene evolution of salt lakes in the Qaidam Basin, Qinghai province, China, *Palaeogeogr. Palaeoclimatol. Palaeoecol.*, *54*(1–4), 87–104, doi:10.1016/0031-0182(86)90119-7.
Komar, P. D. (1980), Modes of sediment transport in channelized water flows with ramifications to the erosion of the Martian outflow channels, *Icarus*, *42*(3), 317–329, doi:10.1016/0019-1035(80)90097-4.
Komatsu, G., P. S. Kumar, K. Goto, Y. Sekine, C. Giri, and T. Matsui (2014), Drainage systems of Lonar crater, India: Contributions to Lonar Lake hydrology and crater degradation, *Planet. Space Sci.*, *95*, 45–55, doi:10.1016/j.pss.2013.05.011
Komatsu, G., and G. G. Ori (2000), Exobiological implications of potential sedimentary deposits on Mars, *Planet. Space Sci.*, *48*(11), 1043–1052, doi:10.1016/S0032-0633(00)00078-7.
Kong, F. J., M. G. Kong, B. Hu, and M. P. Zheng (2013), Meteorological data, surface temperature and moisture conditions at the Dalangtan Mars analogous site, in Qinghai Tibet Plateau, China, *44th Lunar and Planetary Science Conference*, Abstract 1743, Texas.
Kong, W. G., M. P. Zheng, F. J. Kong, and W. X. Chen (2014), Sulfate-bearing deposits at Dalangtan playa and their implication for the formation and preservation of Martian salts, *Am. Mineral.*, *99*(2–3), 283–290, doi:10.2138/am.2014.4594.
Kong, W. G., M. P. Zheng, F. J. Kong, A. Wang, W. X. Chen, and B. Hu (2013), Sedimentary salts at Dalangtan playa and its implications for the formation and preservation of Martian salts, Abstract 1336 presented at the 40th Lunar and Planetary Science Conference, Texas.
Laity, J. E., and N. T. Bridges (2013), Abraded systems, in *Treatise on Geomorphology*, vol. 11, edited by J. F. Shroder et al., pp. 169–286, Academic Press, San Diego, Calif.
Lancaster, N. (2009), Dune morphology and dynamics, in *Geomorphology of Desert Environments*, edited by A. Parsons and A. Abrahams, pp. 557–595, Springer, Dordrecht, Netherlands.
Landheim, R., M. Geringer, R. Greeley, and J. Barker (1992), Radar-visible wind streaks on Venus compared with terrestrial analogs, *43th Lunar and Planetary Science Conference*, Abstract 23, 755.
Lee, P., C. S. Cockell, M. M. Marinova, C. P. McKay, and J. W. Rice Jr. (2001), Snow and ice melt flow features on Devon Island, Nunavut, Arctic Canada as possible analogs for recent slope flow features on Mars, *32nd Lunar and Planetary Science Conference*, Abstract 1809, Texas.
Levy, J. (2012), Hydrological characteristics of recurrent slope lineae on Mars: Evidence for liquid flow through regolith and comparisons with Antarctic terrestrial analogs, *Icarus*, *219*(1), 1–4, doi:10.1016/j.icarus.2012.02.016.
Levy, J., J. Head, and D. Marchant (2009a), Thermal contraction crack polygons on Mars: Classification, distribution, and climate implications from HiRISE observations, *J. Geophys. Res.*, *114*, E01007, doi:10.1029/2008JE003273.
Levy, J., J. Head, D. Marchant, J. Dickson, and G. Morgan (2009b), Geologically recent gully–polygon relationships on Mars: Insights from the Antarctic dry valleys on the roles of permafrost, microclimates, and water sources for surface flow, *Icarus*, *201*(1), 113–126, doi:10.1016/j.icarus.2008.12.043.
Levy, J., J. W. Head, D. R. Marchant, J. L. Dickson, and G. A. Morgan (2009c), Geologically recent gully-polygon relationships on Mars: Insights from the Antarctic dry valleys on the roles of permafrost, microclimates, and water sources for surface flow, *Icarus*, *201*(1), doi:10.1016/j.icarus.2008.1012.1043.
Levy, J., J. W. Head, and D. R. Marchant (2011), Gullies, polygons and mantles in Martian permafrost environments: Cold desert landforms and sedimentary processes during recent Martian geological history, *Geol. Soc. Spec. Publ.*, *354*(1), 167–182, doi:10.1144/SP354.10.
Li, J., Z. B. Dong, G. Q. Qian, Z. C. Zhang, W. Y. Luo, J. F. Lu, and M. Wang (2016), Yardangs in the Qaidam Basin, northwestern China: Distribution and morphology, *Aeolian Res.*, *20*, 89–99, doi:10.1016/j.aeolia.2015.11.002.
Livingstone, I., G. Wiggs, and C. Weaver (2007), Geomorphology of desert sand dunes: A review of recent progress, *Earth Sci. Rev.*, *80*, 239–257, doi:10.1016/j.earscirev.2006.09.004.
Lowestein, T. K., and L. A. Hardie (1985), Criteria for the recognition of salt-pan evaporates, *Sedimentology*, *32*(5), 627–644.
Malin, M. C., and K. S. Edgett (2000a), Sedimentary rocks of early Mars, *Science*, *290*(5498), 1927–1937, doi:10.1126/science.290.5498.1927.

Malin, M. C., and K. S. Edgett (2000b), Evidence for recent groudwater seepage and surface runoff on Mars, *Science*, *288*(5475), 2330–2335, doi:10.1126/science.288.5475.2330.
Malin, M. C., and K. S. Edgett (2001), Mars Global Surveyor Mars Orbiter Camera: Interplanetary cruise throught primary mission, *J. Geophys. Res.*, *106*, 23429–23570, doi:10.1029/2000JE001455.
Malin, M. C., et al. (1998), Early views of the Martian surface from the Mars orbiter camera of Mars global surveyor, *Science*, *279*(5357), 1681–1685, doi:10.1126/science.279.5357.1681.
Mandt, K. E., S. L. De Silva, J. R. Zimbelman, and D. A. Crown (2008), Origin of the Medusae Fossae formation, Mars: Insights from a synoptic approach, *J. Geophys. Res.*, *113*, E12011, doi:10.1029/2008JE003076.
Mangold, N., F. Costard, and F. Forget (2003), Debris flows over sand dunes on Mars: Evidence for liquid water, *J. Geophys. Res.*, *108*, 5027, doi:10.1029/2002JE001958.
Marchant, D. R., and J. W. Head (2007), Antarctic dry valleys: Microclimate zonation, variable geomorphic processes, and implications for assessing climate change on Mars, *Icarus*, *192*(1), 187–222, doi:10.1016/j.icarus.2007.06.018.
Masursky, H., J. Boyce, A. Dial, G. Schaber, and M. Strobell (1977), Classification and time of formation of Martian channels based on Viking data, *J. Geophys. Res.*, *82*, 4016–4038, doi:10.1029/JS082i028p04016.
Mayer, D., R. Arvidson, A. Wang, P. Sobron, and M. Zheng (2009), Mapping minerals at a potential Mars analogue site on the Tibetan Plateau, *40th Lunar and Planetary Science Conference*, Abstract 1877.
McEwen, A. S., C. M. Dundas, S. S. Mattson, A. D. Toigo, L. Ojha, J. J. Wray, M. Chojnacki, S. Byrne, S. L. Murchie, and N. Thomas (2014), Recurring slope lineae in equatorial regions of Mars, *Nat. Geosci.*, *7*, 53–58, doi:10.1038/ngeo2014.
McEwen, A. S., L. Ojha, C. M. Dundas, S. S. Mattson, S. Byrne, J. J. Wray, S. C. Cull, S. L. Murchie, N. Thomas, and V. C. Gulick (2011), Seasonal flows on warm Martian slopes, *Science*, *333*(6043), 740–743, doi:10.1126/science.1204816.
McLennan, S., J. Bell, W. Calvin, P. Christensen, B. Clark, P. De Souza, J. Farmer, W. Farrand, D. Fike, and R. Gellert (2005), Provenance and diagenesis of the evaporite-bearing Burns formation, Meridiani Planum, Mars, *Earth Planet. Sci. Lett.*, *240*(1), 95–121, doi:10.1016/j.epsl.2005.09.041.
Métivier, F., Y. Gaudemer, P. Tapponnier, and B. Meyer (1998), Northeastward growth of the Tibet plateau deduced from balanced reconstruction of two depositional areas: The Qaidam and Hexi Corridor basins, China, *Tectonics*, *17*(6), 823–842, doi:10.1029/98TC02764.
Meyer, B., P. Tapponnier, L. Bourjot, F. Metivier, Y. Gaudemer, G. Peltzer, G. Shunmin, and C. Zhitai (1998), Crustal thickening in Gansu-Qinghai, lithospheric mantle subduction, and oblique, strike-slip controlled growth of the Tibet plateau, *Geophys. J. Int.*, *135*(1), 1–47, doi:10.1046/j.1365-246X.1998.00567.x.
Moore, J. M., and K. S. Edgett (1993), Hellas Planitia, Mars-site of net dust erosion and implications for the nature of basin floor deposits, *Geophys. Res. Lett.*, *20*, 1599–1602, doi:10.1029/93GL01302.
Moore, J. M., and A. D. Howard (2005), Large alluvial fans on Mars, *J. Geophys. Res.*, *110*, E04005, doi:10.1029/2004JE002352.
Moore, J. M., and D. E. Wilhelms (2001), Hellas as a possible site of ancient ice-covered lakes on Mars, *Icarus*, *154*(2), 258–276, doi:10.1006/icar.2001.6736.
Munyikwa, K. (2005), The role of dune morphogenetic history in the interpretation of linear dune luminescence chronologies: A review of linear dune dynamics, *Prog. Phys. Geogr.*, *29*, 317–336, doi:10.1191/0309133305pp451ra.
Murchie, S., et al. (2009), Evidence for the origin of layered deposits in Candor Chasma, Mars, from mineral composition and hydrologic modeling, *J. Geophys. Res.*, 114, E00D05, doi:10.1029/2009JE003343.
Navarro-González, R., et al. (2003), Mars-like soils in the Atacama Desert, Chile, and the dry limit of microbial life, *Science*, *302*(5647), 1018–1021, doi:10.1126/science.1089143.
Ojha, L., M. B. Wilhelm, S. L. Murchie, A. S. McEwen, J. J. Wray, J. Hanley, M. Masse, and M. Chojnacki (2015), Spectral evidence for hydrated salts in recurring slope lineae on Mars, *Nat. Geosci.*, *8*, 829–832, doi:10.1038/ngeo2546.
Osinski, G. (2007), The geology of Mars: Evidence from Earth-based analogs, edited by M. G. Chapman, *Meteorit. Planet. Sci.*, *42*(10), 1855–1856, doi:10.1111/j.1945-5100.2007.tb00543.x.
Paillou, P., and A. Rosenqvist (2003), A JERS-1 radar mosaic for subsurface geology mapping in East Sahara, *Geoscience and Remote Sensing Symposium*, 2003, IGARSS'03 Proceedings, 2003 IEEE International, 1870–1872, doi:10.1109/IGARSS.003.1294277.
Parteli, E., O. Duran, H. Tsoar, V. Schwammle, and H. Herrmann (2009), Dune formation under bimodal winds, *Proc. Natl. Acad. Sci. U.S.A.*, *106*, 22,085–22,089, doi:10.1073/pnas.0808646106.
Pollack, J. B., D. S. Colburn, F. M. Flasar, R. Kahn, C. E. Carlston, and D. Pidek (1979), Properties and effects of dust particles suspended in the Martian atmosphere, *J. Geophys. Res.*, *84*, 2929–2945.
Pollard, W., T. Haltigin, L. Whyte, T. Niederberger, D. Andersen, C. Omelon, J. Nadeau, M. Ecclestone, and M. Lebeuf (2009), Overview of analogue science activities at the McGill Arctic Research Station, Axel Heiberg Island, Canadian High Arctic, *Planet. Space Sci.*, *57*(5), 646–659, doi:10.1016/j.pss.2009.01.008.
Qi, H., and H. Fengqing (2007), *Salt Lake Evolution and Paleoclimate Fluctuation in Qaidam Basin*, pp. 52–201, Science Press, Beijing.
Read, P. L., and S. R. Lewis (2004), *The Martian Climate Revisited: Atmosphere and Environment of a Desert Planet*, pp. 179–247, Springer Science & Business Media, Berlin.
Rice, M., J. Bell, E. Cloutis, A. Wang, S. Ruff, M. Craig, D. T. Bailey, J. R. Johnson, P. A. de Souza Jr, and W. Farrand (2010), Silica-rich deposits and hydrated minerals at Gusev crater, Mars: Vis-NIR spectral characterization and regional mapping, *Icarus*, *205*(2), 375–395, doi:10.1016/j.icarus.2009.03.035.
Rodríguez, J. A. P., K. L. Tanaka, A. Yamamoto, D. C. Berman, J. R. Zimbelman, J. S. Kargel, S. Sasaki, Y. Jinguo, and H. Miyamoto (2010), The sedimentary and dynamics of crater-affiliated wind streaks in western Arabia Terra, Mars and Patagonia, Argentina, *Geomorphology*, *121*(1), 30–54, doi:10.1016/j.geomorph.2009.07.020.
Rohrmann, A., R. Heermance, P. Kapp, and F. Cai (2013), Wind as the primary driver of erosion in the Qaidam Basin, China, *Earth Planet. Sci. Lett.*, *374*, 1–10, doi:10.1016/j.epsl.2013.03.011.
Rubin, D. (1990), Lateral migration of linear dunes in the Strzelecki Desert, Australia, *Earth Surf. Process. Landf.*, *15*, 1–14, doi:10.1002/esp.3290150102.
Rubin, D., and P. Hesp (2009), Multiple origins of linear dunes on Earth and Titan, *Nat. Geosci.*, *2*, 653–658, doi:10.1038/ngeo610.
Sagan, C., J. Veverka, P. Fox, R. Dubisch, J. Lederberg, E. Levinthal, L. Quam, R. Tucker, J. B. Pollack, and B. A. Smith (1972), Variable features on Mars: Preliminary Mariner 9 television results, *Icarus*, *17*(2), 346–372, doi:10.1016/0019-1035(72)90005-X.
Schlesinger, W. H., J. S. Pippen, M. D. Wallenstein, K. S. Hofmockel, D. M. Klepeis, and B. E. Mahall (2003), Community composition and photosynthesis by photoautotrophs under quartz pebbles, southern Mojave Desert, *Ecology*, *84*(12), 3222–3231, doi:10.1890/02-0549.
Squyres, S. W., et al. (2004), In situ evidence for an ancient aqueous environment at Meridiani Planum, Mars, *Science*, *306*(5702), 1709–1714, doi:10.1126/science.1104559.

Szabo, T., G. Domokos, J. P. Grotzinger, and D. J. Jerolmack (2015), Reconstructing the transport history of pebbles on Mars, *Nat. Commun.*, *6*(8366), doi:10.1038/ncomms9366.
Tapponnier, P., X. Zhiqin, F. Roger, B. Meyer, N. Arnaud, G. Wittlinger, and Y. Jingsui (2001), Oblique stepwise rise and growth of the Tibet Plateau, *Science*, *294*(5547), 1671–1677, doi:10.1126/science.105978.
Thomas, D. S. (2011), *Arid Zone Geomorphology: Process, Form and Change in Drylands*, pp. 61–79, John Wiley, Oxford, U. K.
Thomas, P., and J. Veverka (1979), Seasonal and secular variation of wind streaks on Mars: An analysis of Mariner 9 and Viking data, *J. Geophys. Res.*, *84*, 8131–8146, doi:10.1029/JB084iB14p08131.
Thomas, P., J. Veverka, S. Lee, and A. Bloom (1981), Classification of wind streaks on Mars, *Icarus*, *45*(1), 124–153, doi:10.1016/0019-1035(81)90010-5.
Thomas, P., J. Veverka, D. Gineris, and L. Wong (1984), Dust streaks on Mars, *Icarus*, *60*, 161–179, doi:10.1016/0019-1035(84)90145-3.
Tokano, T. (2010), Dune-forming winds on Titan and the influence of topography, *Aeolian Res.*, *2*, 113–127, doi:10.1016/j.aeolia.2010.04.003.
Tsoar, H. (1989), Linear dunes—Forms and formations, *Prog. Phys. Geogr.*, *13*, 507–528, doi:10.1177/030913338901300402.
Tsoar, H., D. Blumberg, and Y. Stoler (2004), Elongation and migration of sand dunes, *Geomorphology*, *57*, 293–302, doi:10.1016/S0169-555X(03)00161-2.
Van der Merwe, E., C. Strydom, and J. Potgieter (1999), Thermogravimetric analysis of the reaction between carbon and $CaSO_4 \cdot 2H_2O$, gypsum and phosphogypsum in an inert atmosphere, *Thermochim. Acta*, *340*, 431–437, doi:10.1016/S0040-6031(99)00287-7.
Veverka, J., P. Gierasch, and P. Thomas (1981), Wind streaks on Mars—Meteorological control of occurrence and mode of formation, *Icarus*, *45*, 154–166, doi:10.1016/0019-1035(81)90011-7.
Wang, A., and M. Zheng (2009), Evaporative salts from saline lakes on Tibetan Plateau: An analog for salts on Mars, *40th Lunar and Planetary Science Conference*, Abstract 1858.
Wang, J., X. Fang, E. Appel, and W. Zhang (2013), Magnetostratigraphic and radiometric constraints on salt formation in the Qaidam Basin, NE Tibetan Plateau, *Quat. Sci. Rev.*, *78*, 53–64, doi:10.1016/j.quascirev.2013.07.017.
Ward, A. (1979), Yardangs on Mars: Evidence of recent wind erosion, *J. Geophys. Res.*, *84*, 8147–8166, doi:10.1029/JB084iB14p08147.
Wei, X., C. Shao, M. Wang, D. Zhao, K. Cai, J. Jiang, G. He, and W. Hu (1993), *Material Constituents, Depositional Features and Formation Conditions of Potassium-Rich Salt Lakes in Western Qaidam Basin*, pp. 26–41, Geological Publishing House, Beijing.
Wierzchos, J., C. Ascaso, and C. P. McKay (2006), Endolithic cyanobacteria in halite rocks from the hyperarid core of the Atacama Desert, *Astrobiology*, *6*(3), 415–422, doi:10.1089/ast.2006.6.415.
Williams, R. M. E., et al. (2013), Martian fluvial conglomerates at Gale Crater, *Science*, *340*(6136), 1068–1072, doi:10.1126/science.1237317.
Wray, J. J. (2013), Gale Crater: The Mars Science Laboratory/Curiosity rover landing site, *Astrobiology*, *12*(01), 25–38, doi:10.1017/S1473550412000328.
Wynn-Williams, D. D. (2000), Cyanobacteria in deserts-life at the limit?, in *The Ecology of Cyanobacteria—Their Diversity in Time and Space*, edited by B. A. Whitton, and M. Potts, pp. 341–366, Kluwer Acad., Dordrecht, Netherlands.
Xiao, L., J. Wang, Y. Dang, Z. Cheng, T. Huang, J. Zhao, Y. Xu, J. Huang, Z. Xiao, and G. Komatsu (2016), A new terrestrial analogue site for Mars research: The Qaidam Basin, Tibetan Plateau (NW China), *Earth Sci. Rev.*, *164*, 84–101, doi:10.1016/j.earscirev.2016.11.003.
Yin, A., Y. Q. Dang, L. C. Wang, W. M. Jiang, S. P. Zhou, X. H. Chen, G. E. Gehrels, and M. W. McRivette (2008), Cenozoic tectonic evolution of Qaidam basin and its surrounding regions (part1): The southern Qilian Shan-Nan Shanthrust belt and northern Qaidam basin, *Geol. Soc. Am. Bull.*, *120*(7–8), 813–846, doi:10.1130/B26180.1.
Yingst, R. A., et al. (2013), Characteristics of pebble-and cobble-sized clasts along the Curiosity rover traverse from Bradbury landing to Rocknest, *J. Geophys. Res. Planets*, *118*, 2361–2380, doi:10.1002/2013JE004435.
Yu, J. Q., C. L. Gao, A. Y. Cheng, Y. Liu, L. Zhang, and X. H. He (2013), Geomorphic, hydroclimatic and hydrothermal controls on the formation of the lithium brine deposits in the Qaidam Basin, northern Tibetan Plateau, China, *Ore Geol. Rev.*, *50*, 171–183, doi:10.1016/j.oregeorev.2012.11.001.
Yu, L., Z. Dong, Z. Lai, G. Qian, and T. Pan (2015), Origin and lateral migration of linear dunes in the Qaidam Basin of NW China revealed by dune sediments, internal structures, and optically stimulated luminescence ages, with implications for linear dunes on Titan: Comment and discussion, *Geol. Soc. Am. Bull.*, *127*(1–2), 316–320, doi:10.1130/B31041.1.
Zheng, M., W. Kong, X. Zhang, W. Chen, and F. Kong (2013), A comparative analysis of evaporate sediments on Earth and Mars: Implications for the climate change on Mars, *Acta Geol. Sin. (English Ed.)*, *87*(3), 885–897, doi:10.1111/1755-6724.12096.
Zheng, M., A. Wang, F. Kong, and N. Ma (2009), Saline lakes on Qinghai-Tibet Plateau and salts on Mars, *40th Lunar and Planetary Science Conference*, Abstract 1454.
Zheng, M. P. (1997), *An Introduction to Saline Lakes on the Qinghai-Tibet Plateau*, pp. 23–48, Kluwer Acad., Dordrecht, Netherlands.
Zheng, M. P., T. Jiayou, L. Junying, and Z. Fasheng (1993), Chinese saline lakes, *Hydrobiologia*, *267*(1), 23–36, doi:10.1007/BF00018789.
Zhou, J. X., Y. Zhu, and C. Q. Yuan (2012), Origin and lateral migration of linear dunes in the Qaidam Basin of NW China revealed by dune sediments, internal structures, and optically stimulated luminescence ages, with implications for linear dunes on Titan, *Geol. Soc. Am. Bull.*, *124*(7–8), 1147–1154, doi:10.1130/B30550.1.
Zimbelman, J. R. (1986), Surface properties of the Pettit wind streak on Mars: Implications for sediment transport, *Icarus*, *66*(1), 83–93, doi:10.1016/0019-1035(86)90008-4.
Zimbelman, J. R., and S. Williams (1996), Wind streaks: Geological and botanical effects on surface albedo contrast, *Geomorphology*, *17*(1–3), 167–185, doi:10.1016/0169-555X(95)00098-P.
Zimbelman, J. R., M. C. Bourke, and R. D. Lorenz (2013), Recent developments in planetary Aeolian studies and their terrestrial analogs, *Aeolian Res.*, *11*, 109–126, doi:10.1016/j.aeolia.2013.04.004.